Inorganic Chemistry
Article

*Inorg. Chem.* **2010**, *49*, 10117–10132 **10117**
DOI: 10.1021/ic101399k

# Models for the Active Site in [FeFe] Hydrogenase with Iron-Bound Ligands Derived from Bis-, Tris-, and Tetrakis(mercaptomethyl)silanes

**Ulf-Peter Apfel,[†] Dennis Troegel,[‡] Yvonne Halpin,[§] Stefanie Tschierlei,[∥] Ute Uhlemann,[∥] Helmar Görls,[†] Michael Schmitt,[∥] Jürgen Popp,[∥] Peter Dunne,[⊥] Munuswamy Venkatesan,[⊥] Michael Coey,*[,⊥] Manfred Rudolph,*[,†] Johannes G. Vos,*[,§] Reinhold Tacke,*[,‡] and Wolfgang Weigand*[,†]**

[†]*Institut für Anorganische und Analytische Chemie, Friedrich-Schiller-Universität Jena, August-Bebel-Strasse 2, D-07743 Jena, Germany,* [‡]*Institut für Anorganische Chemie, Universität Würzburg, Am Hubland, D-97074 Würzburg, Germany,* [§]*Solar Energy Conversion SRC, School of Chemical Sciences, Dublin City University, Dublin 9, Ireland,* [∥]*Institut für Physikalische Chemie, Friedrich-Schiller-Universität Jena, Helmholtzweg 4, D-07743 Jena, Germany, and Institut für Photonische Technologien, Friedrich-Schiller-Universität Jena, Albert-Einstein-Strasse 9, D-07745 Jena, Germany, and* [⊥]*SFI-Trinity Nanoscience Laboratory, Physics Department, Trinity College, Dublin 2, Ireland*

Received July 14, 2010

A series of multifunctional (mercaptomethyl)silanes of the general formula type $R_nSi(CH_2SH)_{4-n}$ ($n$ = 0−2; R = organyl) was synthesized, starting from the corresponding (chloromethyl)silanes. They were used as multidentate ligands for the conversion of dodecacarbonyltriiron, $Fe_3(CO)_{12}$, into iron carbonyl complexes in which the deprotonated (mercaptomethyl)silanes act as $\mu$-bridging ligands. These complexes can be regarded as models for the [FeFe] hydrogenase. They were characterized by elemental analyses (C, H, S), NMR spectroscopic studies ($^1$H, $^{13}$C, $^{29}$Si), and single-crystal X-ray diffraction. Their electrochemical properties were investigated by cyclic voltammetry to disclose a new mechanism for the formation of dihydrogen catalyzed by these compounds, whereby one sulfur atom was protonated in the catalytic cycle. The reaction of the tridentate ligand $MeSi(CH_2SH)_3$ with $Fe_3(CO)_{12}$ yielded a tetranuclear cluster compound. A detailed investigation by X-ray diffraction, electrochemical, Raman, Mössbauer, and susceptibility techniques indicates that for this compound initially $[Fe_2\{\mu\text{-}MeSi(CH_2S)_2CH_2SH\}(CO)_6]$ is formed. This dinuclear complex, however, is slowly transformed into the tetranuclear species $[Fe_4\{\mu\text{-}MeSi(CH_2S)_3\}_2(CO)_8]$.

## Introduction

Since Peters et al.[1] and Fontecilla-Camps et al.[2] have determined the structure of the [FeFe]-hydrogenases' active site, much effort was made to mimic the properties of the enzyme.[3] Especially the protonation features of model complexes, namely, the formation of terminal and bridging hydrides as well as a possible shift of protons to the diiron core via adjacent bases, has been the focus of many investigations.[4] Whereas the propanedithiolato complex $[Fe_2(\mu\text{-pdt})(CO)_6]$ reveals addition of a proton to the diiron center and formation of a hydride,[5] the azadithiolato complex $[Fe_2(\mu\text{-adt})(CO)_6]$ shows first protonation of the amino group and consecutive shift of this proton to an iron atom, forming a terminal hydride.[6] Recently, alkylation[7] as well as oxidation[8] of the thiolato sulfur atoms in [FeFe] hydrogenase model complexes was reported and confirmed the high reactivity of the thiolato sulfur atoms. However, Darensbourg et al.

*To whom correspondence should be addressed. E-mail: jcoey@tcd.ie (M.C.), manfred.rudolph@uni-jena.de (M.R.), han.vos@dcu.ie (J.G.V.), r.tacke@uni-wuerzburg.de (R.T.), wolfgang.weigand@uni-jena.de (W.W.).

(1) Peters, J. W.; Lanzilotta, W. N.; Lemon, B. J.; Seefeldt, L. C. *Science* **1998**, *282*, 1853–1858.

(2) Nicolet, Y.; Piras, C.; Legrand, P.; Hatchikian, C. E.; Fontecilla-Camps, J. C. *Structure* **1999**, *7*, 13–23.

(3) (a) Razavet, M.; Davies, S. C.; Hughes, D. L.; Pickett, C. J. *Chem. Commun.* **2001**, 847–848. (b) Razavet, M.; Davies, S. C.; Hughes, D. L.; Barclay, J. E.; Evans, D. J.; Fairhurst, S. A.; Liu, X.; Pickett, C. J. *Dalton Trans.* **2003**, 586–595. (c) Tard, C.; Liu, X.; Ibrahim, S. K.; Bruschi, M.; De Gioia, L.; Davies, S. C.; Yang, X.; Wang, L.-S.; Sawers, G.; Pickett, C. J. *Nature* **2005**, *433*, 610–613. (d) Song, L.-C.; Cheng, J.; Yan, J.; Wang, H.-T.; Liu, X.-F.; Hu, Q.-M. *Organometallics* **2006**, *25*, 1544–1547. (e) Windhager, J.; Görls, H.; Petzold, H.; Mloston, G.; Linti, G.; Weigand, W. *Eur. J. Inorg. Chem.* **2007**, 4462–4471. (f) Apfel, U.-P.; Halpin, Y.; Gottschaldt, M.; Görls, H.; Vos, J. G.; Weigand, W. *Eur. J. Inorg. Chem.* **2008**, 5112–5118. (g) Song, L.-C.; Fang, X.-N.; Li, C.-G.; Yan, J.; Bao, H.-L.; Hu, Q.-M. *Organometallics* **2008**, *27*, 3225–3231. (h) Singleton, M. L.; Bhuvanesh, N.; Reibenspies, J. H.; Darensbourg, M. Y. *Angew. Chem.* **2008**, *120*, 9634–9637. *Angew. Chem., Int. Ed.* **2008**, *47*, 9492−9495. (i) Apfel, U.-P.; Kowol, C. R.; Halpin, Y.; Kloss, F.; Kübel, J.; Görls, H.; Vos, J. G.; Keppler, B. K.; Morera, E.; Lucente, G.; Weigand, W. *J. Inorg. Biochem.* **2009**, *103*, 1236–1244. (j) Harb, M. K.; Apfel, U.-P.; Kübel, J.; Görls, H.; Felton, G. A. N.; Sakamoto, T.; Evans, D. H.; Glass, R. S.; Lichtenberger, D. L.; El-khateeb, M.; Weigand, W. *Organometallics* **2009**, *28*, 6666–6675.

(4) Tard, C.; Pickett, C. J. *Chem. Rev.* **2009**, *109*, 2245–2274, and references cited herein.


Published on Web 09/27/2010

calculated that protonation of the Fe−Fe bond pair should be favored.[7a] In contrast to that report, we investigated the chemical and electrochemical properties of $[Fe_2(\mu\text{-}SCH_2SCH_2S)(CO)_6]$ and observed interaction of pivalic acid with at least one sulfur atom.[9] This might be an alternative pathway for the formation of hydrides via an initial protonation of the thiolato sulfur atoms.

Inspired by these results and investigations of Glass et al. on $[Fe_2\{\mu\text{-}SCH_2Sn(CH_3)_2CH_2S\}(CO)_6]$,[10] which exhibits an increased electron density at the thiolato sulfur atoms by hyperconjugation of the $\sigma$(Sn−C) and 3p(S) orbitals, we have prepared a series of model compounds for the [FeFe] hydrogenase with silicon-containing thiolato ligands bridging the diiron moiety. These complexes should offer the possibility to investigate protonation processes at the coordinating thiolato sulfur atoms by spectroscopic (IR, NMR) as well as electrochemical (cyclic voltammetry, difference pulse voltammetry) techniques.

It is well-known from silicon-containing drugs that the presence of one or more silicon atoms in these molecules influences their chemical, physical, and biological properties.[11] The pharmacodynamics and pharmacokinetics of drugs can be affected significantly by replacement of a carbon by a silicon atom (sila-substitution). This can be exploited in medicinal chemistry for drug design; and indeed, the carbon/silicon switch strategy has been successfully used for the development of new silicon-based drugs. Likewise, sila-substitution of odorants has also been demonstrated to affect their olfactory properties, and the carbon/silicon switch strategy has been successfully used for the development of new silicon-based odorants.[12] Recently, we have also shown that the impact and friction sensitivity of explosives can be affected by carbon/silicon exchange.[13]

The main focus of this work was the synthesis of iron complexes containing silicon-based thiolato ligands derived from (mercaptomethyl)silanes of the formula type $R_nSi(CH_2SH)_{4-n}$ ($n$ = 0−2; R = organyl) and the determination of the electrochemical properties of these complexes (in comparison to the corresponding carbon analogues) to investigate the influence of silicon on electrocatalysis and the formation of dihydrogen. These studies were also performed as part of our systematic investigations on functionalized tetraorganylsilanes of the formula type $R_nSi(CH_2X)_{4-n}$ ($n$ = 0−3; R = organyl; X = functional group).[13,14]

## Results and Discussion

**Synthesis and Characterization of the Silicon-Containing Thiolato Ligands.** The di- and trifunctional (mercaptomethyl)silanes **4a**−**d** were synthesized according to Scheme 1, starting from the respective chlorosilanes **1a**−**d**. Thus, treatment of **1a**−**d** with (chloromethyl)lithium, generated in situ from bromochloromethane and *n*-butyllithium in tetrahydrofuran (THF),[15] afforded the (chloromethyl)-silanes **2a**−**d** (37−77% yield), which upon treatment with potassium thioacetate in THF furnished the corresponding (acetylthiomethyl)silanes **3a**−**d** (77−97% yield). Reaction of **3a**−**d** with lithium aluminum hydride in diethyl ether, followed by workup with hydrochloric acid, finally afforded the respective (mercaptomethyl)silanes **4a**−**d** (67−92% yield). Compounds **2a**−**d**, **3a**−**d**, and **4a**−**d** were isolated as liquids. Their identities were established by elemental analyses (C, H, S) and $^1$H, $^{13}$C, and $^{29}$Si NMR spectroscopic studies (solvent, $CDCl_3$).

**Synthesis and Characterization of the Iron Complexes.** Treatment of the bis(mercaptomethyl)silanes **4a**−**c** with

(5) (a) Borg, S. J.; Behrsing, T.; Best, S. P.; Razavet, M.; Liu, X.; Pickett, C. J. *J. Am. Chem. Soc.* **2004**, *126*, 16988–16999. (b) Chong, D. S.; Georgakaki, I. P.; Mejia-Rodriguez, R.; Sanabria- Chinchilla, J.; Soriaga, M. P.; Darensbourg, M. Y. *Dalton Trans.* **2003**, 4158–4163.

(6) (a) Capon, J.-F.; Ezzaher, S.; Gloaguen, F.; Pétillon, F. Y.; Schollhammer, P.; Talarmin, J. *Chem.—Eur. J.* **2008**, *14*, 1954–1964. (b) Olsen, M. T.; Barton, B. E.; Rauchfuss, T. B. *Inorg. Chem.* **2009**, *48*, 7507–7509.

(7) (a) Zhao, X.; Chiang, C.-Y.; Miller, M. L.; Rampersad, M. V.; Darensbourg, M. Y. *J. Am. Chem. Soc.* **2003**, *125*, 518–524. (b) Tye, J. W.; Darensbourg, M. Y.; Hall, M. B. *J. Mol. Struct.: THEOCHEM* **2006**, *771*, 123–128.

(8) (a) Windhager, J.; Seidel, R. A.; Apfel, U.-P.; Görls, H.; Linti, G.; Weigand, W. *Chem. Biodiversity* **2008**, *5*, 2023–2041. (b) Windhager, J.; Apfel, U.-P.; Yoshino, T.; Nakata, N.; Görls, H.; Rudolph, M.; Ishii, A.; Weigand, W. *Chem. Asian J.* **2010**, *5*, 1600−1610. (c) Liu, T.; Li, B.; Singleton, M. L.; Hall, M. B.; Darensbourg, M. Y. *J. Am. Chem. Soc.* **2009**, *131*, 8296–8307. (d) Li, B.; Liu, T.; Singleton, M. L.; Darensbourg, M. Y. *Inorg. Chem.* **2009**, *48*, 8393–8403.

(9) Windhager, J.; Rudolph, M.; Bräutigam, S.; Görls, H.; Weigand, W. *Eur. J. Inorg. Chem.* **2007**, 2748–2760.

(10) Glass, R. S.; Gruhn, N. E.; Lorance, E.; Singh, M. S.; Stessman, N. Y. T.; Zakai, U. I. *Inorg. Chem.* **2005**, *44*, 5728–5737.

(11) Recent publications dealing with sila-substituted drugs: (a) Showell, G. A.; Barnes, M. J.; Daiss, J. O.; Mills, J. S.; Montana, J. G.; Tacke, R.; Warneck, J. B. H. *Bioorg. Med. Chem. Lett.* **2006**, *16*, 2555–2558. (b) Ilg, R.; Burschka, C.; Schepmann, D.; Wünsch, B.; Tacke, R. *Organometallics* **2006**, *25*, 5396–5408. (c) Büttner, M. W.; Burschka, C.; Daiss, J. O.; Ivanova, D.; Rochel, N.; Kammerer, S.; Peluso-Iltis, C.; Bindler, A.; Gaudon, C.; Germain, P.; Moras, D.; Gronemeyer, H.; Tacke, R. *ChemBioChem* **2007**, *8*, 1688–1699. (d) Tacke, R.; Popp, F.; Müller, B.; Theis, B.; Burschka, C.; Hamacher, A.; Kassack, M. U.; Schepmann, D.; Wünsch, B.; Jurva, U.; Wellner, E. *ChemMedChem* **2008**, *3*, 152–164. (e) Warneck, J. B.; Cheng, F. H. M.; Barnes, M. J.; Mills, J. S.; Montana, J. G.; Naylor, R. J.; Ngan, M.-P.; Wai, M.-K.; Daiss, J. O.; Tacke, R.; Rudd, J. A. *Toxicol. Appl. Pharmacol.* **2008**, *232*, 369–375. (f) Lippert, W. P.; Burschka, C.; Götz, K.; Kaupp, M.; Ivanova, D.; Gaudon, C.; Sato, Y.; Antony, P.; Rochel, N.; Moras, D.; Gronemeyer, H.; Tacke, R. *ChemMedChem* **2009**, *4*, 1143–1152. (g) Tacke, R.; Müller, V.; Büttner, M. W.; Lippert, W. P.; Bertermann, R.; Daiss, J. O.; Khanwalkar, H.; Furst, A.; Gaudon, C.; Gronemeyer, H. *ChemMedChem* **2009**, *4*, 1797–1802. (h) Johansson, T.; Weidolf, L.; Popp, F.; Tacke, R.; Jurva, U. *Drug Metab. Dispos.* **2010**, *38*, 73–83. (i) Tacke, R.; Nguyen, B.; Burschka, C.; Lippert, W. P.; Hamacher, A.; Urban, C.; Kassack, M. U. *Organometallics* **2010**, *29*, 1652–1660.

(12) Recent publications dealing with sila-substituted odorants: (a) Büttner, M. W.; Penka, M.; Doszczak, L.; Kraft, P. *Organometallics* **2007**, *26*, 1295–1298. (b) Doszczak, L.; Kraft, P.; Weber, H.-P.; Bertermann, R.; Triller, A.; Hatt, H.; Tacke, R. *Angew. Chem.* **2007**, *119*, 3431–3436. *Angew. Chem., Int. Ed.* **2007**, *46*, 3367−3371. (c) Büttner, M. W.; Metz, S.; Kraft, P.; Tacke, R. *Organometallics* **2007**, *26*, 3925–3929. (d) Büttner, M. W.; Burschka, C.; Junold, K.; Kraft, P.; Tacke, R. *ChemBioChem* **2007**, *8*, 1447–1454. (e) Büttner, M. W.; Nätscher, J. B.; Burschka, C.; Tacke, R. *Organometallics* **2007**, *26*, 4835–4838. (f) Tacke, R.; Metz, S. *Chem. Biodiversity* **2008**, *5*, 920–941. (g) Metz, S.; Nätscher, J. B.; Burschka, C.; Götz, K.; Kaupp, M.; Kraft, P.; Tacke, R. *Organometallics* **2009**, *28*, 4700–4712. (h) Nätscher, J. B.; Laskowski, N.; Kraft, P.; Tacke, R. *ChemBioChem* **2010**, *11*, 315–319.

(13) Recent publications dealing with sila-substituted explosives: (a) Klapötke, T. M.; Krumm, B.; Ilg, R.; Troegel, D.; Tacke, R. *J. Am. Chem. Soc.* **2007**, *129*, 6908–6915. (b) Evangelisti, C.; Klapötke, T. M.; Krumm, B.; Nieder, A.; Berger, R. J. F.; Hayes, S. A.; Mitzel, N. W.; Troegel, D.; Tacke, R. *Inorg. Chem.* **2010**, *49*, 4865–4880.

(14) Recent publications dealing with functional tetraorganylsilanes of the formula type $R_nSi(CH_2X)_{4-n}$ (R = organyl; X = functional group; $n$ = 0−3): (a) Daiss, J. O.; Bart, K. A.; Burschka, C.; Hey, P.; Ilg, R.; Klemm, K.; Richter, I.; Wagner, S. A.; Tacke, R. *Organometallics* **2004**, *23*, 5193–5197. (b) Ilg, R.; Troegel, D.; Burschka, C.; Tacke, R. *Organometallics* **2006**, *25*, 548–551. (c) Troegel, D.; Walter, T.; Burschka, C.; Tacke, R. *Organometallics* **2009**, *28*, 2756–2761. (d) Troegel, D.; Möller, F.; Burschka, C.; Tacke, R. *Organometallics* **2009**, *28*, 5765–5770. (e) Weidner, T.; Ballav, N.; Siemeling, U.; Troegel, D.; Walter, T.; Tacke, R.; Castner, D. G.; Zharnikov, M. *J. Phys. Chem. C* **2009**, *113*, 19609–19617. (f) Troegel, D.; Lippert, W. P.; Möller, F.; Burschka, C.; Tacke, R. *J. Organomet. Chem.* **2010**, *695*, 1700–1707.

(15) (a) Kobayashi, T.; Pannell, K. H. *Organometallics* **1990**, *9*, 2201–2203. (b) Kobayashi, T.; Pannell, K. H. *Organometallics* **1991**, *10*, 1960–1964.

**Scheme 1.** Syntheses of the Bis(mercaptomethyl)silanes **4a**−**c** and the Tris(mercaptomethyl)silane **4d**

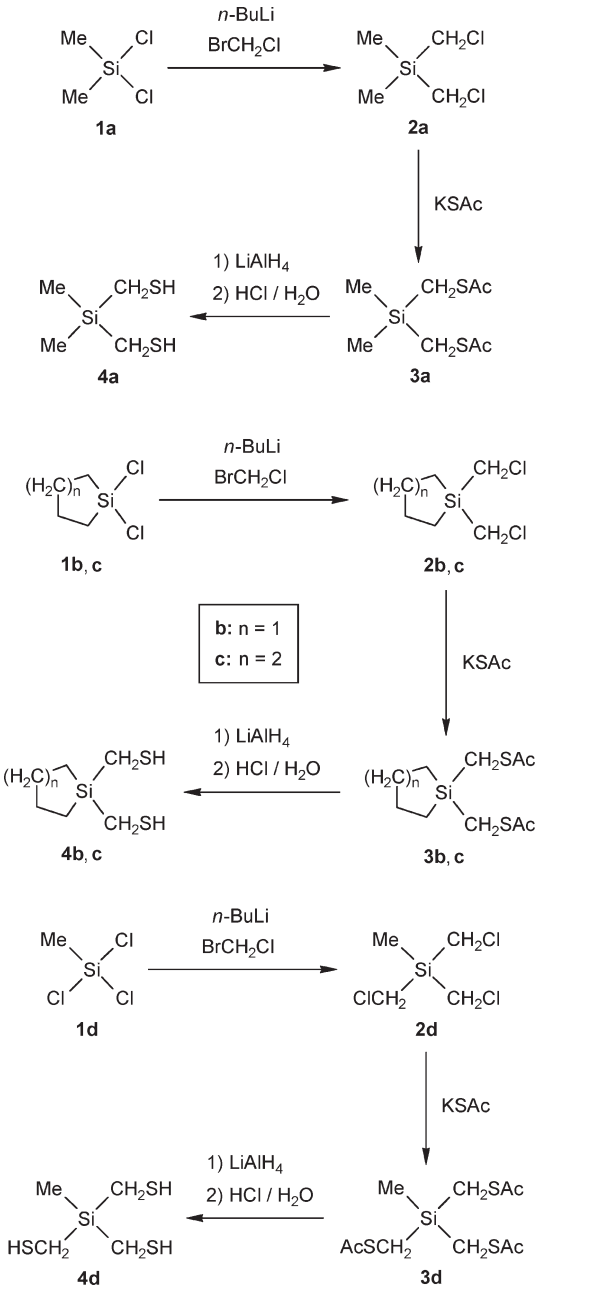


**Scheme 2.** Syntheses of the Diiron Complexes **5a**−**c**

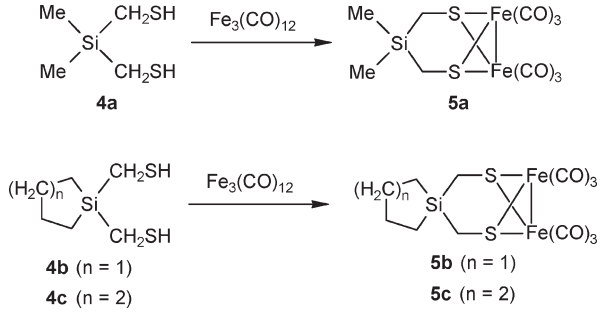


two molar equivalents of dodecacarbonyltriiron, $Fe_3(CO)_{12}$, in toluene afforded the diiron complexes **5a**−**c** (Scheme 2). Compounds **5a**−**c** were isolated in

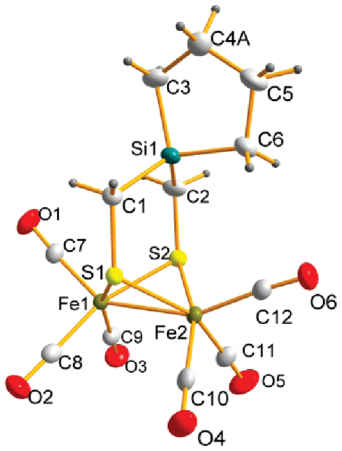


**Figure 1.** Molecular structure of **5b** in the crystal (probability level of displacement ellipsoids 50%).

57−89% yield as red crystalline solids. Their identities were established by elemental analyses (C, H, S), NMR spectroscopic studies ($^1$H, $^{13}$C, $^{29}$Si; solvent, $CDCl_3$), mass-spectrometric investigations, IR spectroscopic studies, and crystal structure analyses (Figure 1; Supporting Information, Figures S1 and S2, Table S1).

As can be seen from Figure 1 as well as Supporting Information, Figures S1 and S2, both iron coordination centers of **5a**−**c** are surrounded by two bridging sulfur atoms, one iron atom, and three carbonyl groups. The iron coordination polyhedra can be best described as strongly distorted octahedra, with the three carbonyl groups in facial positions. The bicyclic [2Fe2S] skeletons of **5a**−**c** display a "butterfly" structure. The silicon atoms of **5a**−**c** are surrounded in a distorted tetrahedral fashion. It is interesting to note that all Si−C−S angles (118.22(12)−122.05(13)°) differ significantly from the ideal tetrahedral angle.

To obtain a [4Fe6S] cluster with two tridentate 3-fold deprotonated $MeSi(CH_2SH)_3$ ligands, the tris(mercaptomethyl)silane **4d** was treated with $Fe_3(CO)_{12}$. Reaction of $Fe_3(CO)_{12}$ with the corresponding carbon-based trithiol, $MeC(CH_2SH)_3$, has already been reported to form the tetrairon complex $[Fe_4\{\mu\text{-}MeC(CH_2S)_3\}_2(CO)_8]$ with an $[Fe^IFe^{II}Fe^{II}Fe^I]$ assembly that catalyzes electrochemical dihydrogen generation at moderate potential.[16] Treatment of the silicon compound **4d** with one molar equivalent of $Fe_3(CO)_{12}$ afforded the diiron complex **6a** (7% yield) and the tetrairon complex **6b** (9% yield) (Scheme 3). The identities of **6a** and **6b** were established by NMR spectroscopic studies ($^1$H, $^{13}$C, $^1$H,$^{13}$C HSQC, $^1$H,$^1$H COSY), mass-spectrometric investigations (FAB-MS), IR and Raman studies, as well as powder X-ray diffractometry. In addition, compound **6b** was structurally characterized by single-crystal X-ray diffraction (Figure 2; Supporting Information, Table S2). Single crystals of **6b** were obtained by slow evaporation of the solvent from a solution of **6a** and **6b** in trichloromethane. It was noticed via powder X-ray diffractometry and thin layer chromatography that **6a** in solution was slowly transformed into **6b**.

(16) (a) Tard, C.; Liu, X.; Hughes, D. L.; Pickett, C. J. *Chem. Commun.* **2005**, 133–135. (b) Cheah, M. H.; Tard, C.; Borg, S. J.; Liu, X.; Ibrahim, S. K.; Pickett, C. J.; Best, S. P. *J. Am. Chem. Soc.* **2007**, *129*, 11085–11092.

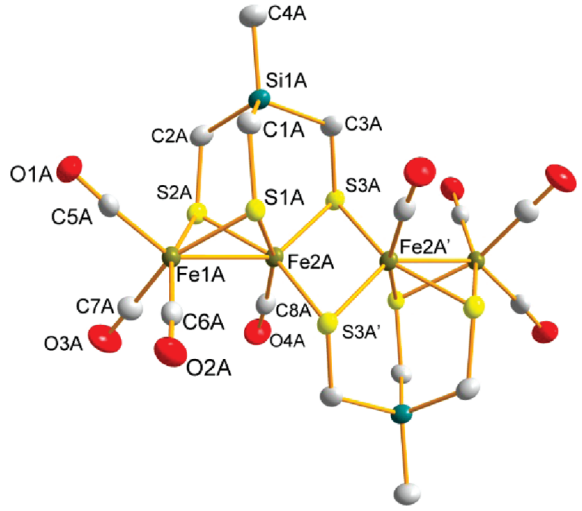


**Figure 2.** Molecular structure of Molecule A in the crystal of **6b** (probability level of displacement ellipsoids 50%). Hydrogen atoms are omitted for clarity.

**Scheme 3.** Syntheses of the Diiron Complex **6a** and the Tetrairon Complex **6b**

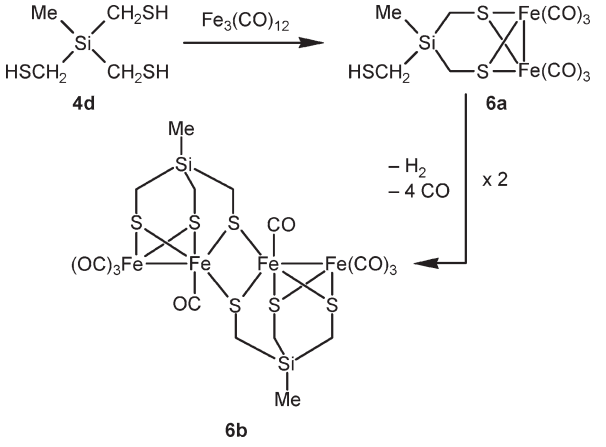


To further prove the presence of a free thiol group and the [$Fe^{I}Fe^{I}$] assembly in **6a**, Raman spectroscopy, Mössbauer, and susceptibility techniques were used. The Raman spectrum of **6a** (Supporting Information, Figure S3) is dominated by methyl and methylene group vibrations, for example, the strong C−H stretching vibration at 2914 $cm^{-1}$, the C−S and C−Si stretching vibrations at 701 $cm^{-1}$, different $CH_3$ and $CH_2$ deformation modes at 1606 and 980 $cm^{-1}$, and the Fe−S stretching vibrations at 513 $cm^{-1}$. The signal at 2593 $cm^{-1}$ is assigned to an S−H stretching mode. In this spectral region, no other vibrational frequencies occur, making this signal a very strong indicator for the existence of an SH group in **6a**.

To obtain further information concerning the structure of **6a** and the redox state of the two iron centers, Mössbauer and susceptibility measurements were carried out for both compound **6a** and the reference compound **5a**. The latter was taken as a well-established example of a [2Fe2S] cluster with an [$Fe^{I}Fe^{I}$] arrangement.

The Mössbauer spectra were fitted by the standard least-squares minimization procedure. The spectrum for **5a** shows a quadrupole doublet with an isomer shift $\delta = -0.04 \pm 0.02$ mm $s^{-1}$ relative to $\alpha_{Fe}$ and a quadrupole splitting $\Delta = 0.78 \pm 0.02$ mm $s^{-1}$ (Table 1, Figure 3). These values are in agreement with those obtained for the structurally related diiron complex [$Fe_2(\mu$-$SCH_2OCH_2S)(CO)_6$][17] ($\delta = -0.02$ mm $s^{-1}$, $\Delta = 0.81$ mm $s^{-1}$). The asymmetry of the spectrum of **5a** indicates the presence of some of the iron atoms (∼ 16%) in a second site giving a doublet with broadened lines and $\delta = 0.19 \pm 0.02$ mm $s^{-1}$ and $\Delta = 0.52 \pm 0.02$ mm $s^{-1}$. Susceptibility measurements on this compound in the liquid helium temperature range showed that less than 1% of the iron atoms in the sample had an unpaired spin. Hence, any unpaired electrons in the low-spin $Fe^{I}$ centers of **5a** are paired to form covalent bonds. Since the covalent bond length expected for a $Fe^{I}$−$Fe^{I}$ bond is 233 pm, the experimentally established Fe−Fe distance of **5a** (252 pm) is in agreement with this interpretation.

**Table 1.** Room-Temperature Mössbauer Data for Compounds **5a** and **6a**

| compound | isomer shift [mm $s^{-1}$] | quadrupole splitting [mm $s^{-1}$] | line width [mm $s^{-1}$] | relative area [%] |
|---|---|---|---|---|
| **5a** | −0.04(2) | 0.78(2) | 0.11(1) | 84 |
| | 0.19(2) | 0.52(2) | 0.34(2) | 16 |
| **6a** | −0.04(2) | 0.82(2) | 0.11(1) | 93 |
| | 0.17(4) | 0.51(4) | 0.42(4) | 7 |

The Mössbauer spectrum of compound **6a** is similar to that of **5a** (Table 1, Figure 3). The main doublet again has a negative isomer shift $\delta = -0.04 \pm 0.02$ mm $s^{-1}$ and a quadrupole splitting $\Delta = 0.82 \pm 0.02$ mm $s^{-1}$, and the minority site (∼ 7% of the iron atoms) gives a doublet with broadened lines and $\delta = 0.17 \pm 0.04$ mm $s^{-1}$ and $\Delta = 0.51 \pm 0.04$ mm $s^{-1}$. The Curie-law susceptibility data in this case is consistent with 8% of the iron atoms possessing a spin of 1/2, or 1% of the iron atoms being present as high-spin $Fe^{II}$ centers (Supporting Information, Figure S4). The spins of the iron atoms are coupled antiferromagnetically.

These investigations further confirmed the identity of compound **6a**. On the basis of the Raman spectrum and the Mössbauer spectra, the presence of a non-coordinated thiol group can be assumed. A coordination of the thiol group to the iron center should lead to both a shift of $\nu_{SH}$ to lower wavenumbers and a significant difference in the quadrupole splitting because of the different coordination sphere of the distal and the proximal iron site.

Compound **6b** crystallizes in the space group $P\bar{1}$, with two molecules (Molecules A and B) in the asymmetric unit, which display very similar centrosymmetric structures. As shown for Molecule A in Figure 2, the tetrairon complex **6b** is a centrosymmetric [4Fe6S] cluster, with two [2Fe3S] cores that are connected via two bridging thiolato groups; that is, the two tripodal S,S,S ligands derived from **4d** are 3-fold deprotonated. The terminal iron coordination centers Fe1A and Fe1A′ are surrounded each by two bridging sulfur atoms (S1A/S2A, S1A′/S2A′), one of the two internal iron atoms (Fe2A, Fe2A′), and three carbonyl groups. The internal iron coordination centers Fe2A and Fe2A′ are each surrounded by four bridging sulfur atoms (S1A/S2A/S3A/S3A′, S1A′/S2A′/S3A′/S3A), one of the two terminal iron atoms (Fe1A, Fe1A′), and one carbonyl group. All four iron coordination polyhedra

(17) Song, L.-C.; Yang, Z.-Y.; Bian, H.-Z.; Hu, Q.-M. *Organometallics* **2004**, *23*, 3082–3084.

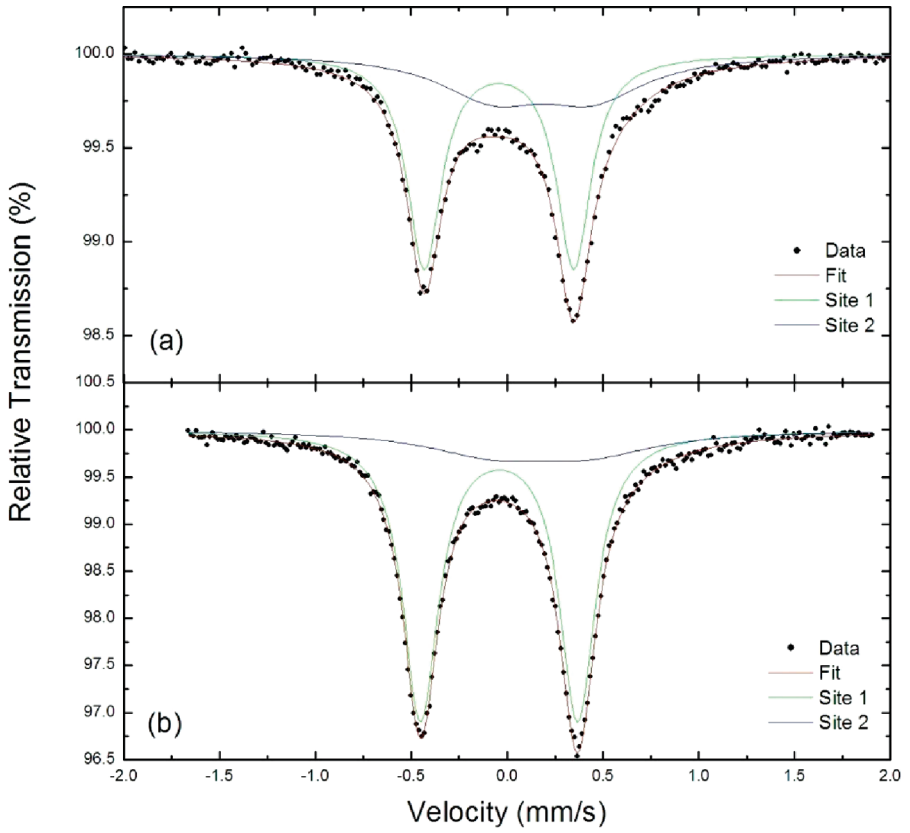


**Figure 3.** Room-temperature Mössbauer spectra for compounds (a) **5a** and (b) **6a**. The fit parameters for the quadrupole doublets are shown in Table 1.

**Scheme 4.** Synthesis of the Tetrairon Complex **7**

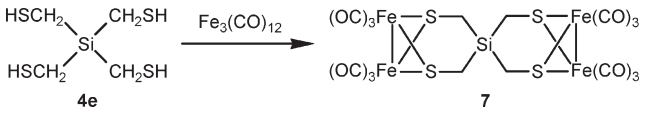


are best described as strongly distorted octahedra. The central Fe2A···Fe2A′ distance (262.84(8) pm) is significantly longer than the Fe1A−Fe2A and Fe1A′−Fe2A′ distances (252.97(6) pm). As also observed for compounds **5a**−**c**, the two bicyclic [2Fe2S] skeletons of **6b** display a "butterfly" structure. The silicon atoms of **6b** are surrounded in a distorted tetrahedral fashion; the Si−C−S angles amount to 111.71(16) (Si1A−C1A−S1A, Si1A′−C1A′−S1A′), 116.91(16) (Si1A−C2A−S2A, Si1A′−C2A′−S2A′), and 116.10(16)° (Si1A−C3A−S3A, Si1A′−C3A′−S3A′), respectively. The structure of **6b** is very similar to that reported for the related compound $[Fe_4\{\mu\text{-MeC}(CH_2S)_3\}_2(CO)_8]$ with its $[Fe^{I}Fe^{II}Fe^{II}Fe^{I}]$ arrangement.[16]

To study the coordination mode of tetrakis(mercaptomethyl)silane (**4e**), this compound was also treated with $Fe_3(CO)_{12}$. With this tetrafunctional ligand, a large number of different types of iron complexes can be expected. However, in our studies, only one compound, namely, the tetrairon complex **7**, could be isolated, and no coordination polymers or charged complexes were found. In contrast to the described synthesis of the carbon analogue of **7**, $[Fe_4\{\mu\text{-C}(CH_2S)_4\}(CO)_{12}]$,[3g] the silicon compound **7** was obtained in the absence of triethylamine by direct conversion of $Fe_3(CO)_{12}$ with **4e** (molar ratio, 2:1) in refluxing toluene (40% yield) (Scheme 4). Variation of the molar ratio of $Fe_3(CO)_{12}$:**4e** to 1:1 should lead to the

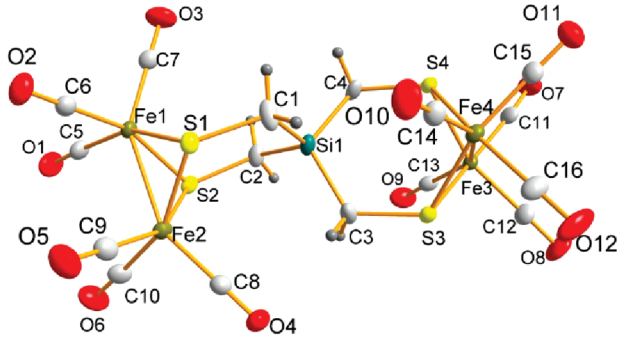


**Figure 4.** Molecular structure of **7** in the crystal (probability level of displacement ellipsoids 50%).

diiron complex $[Fe_2\{\mu\text{-SCH}_2\text{Si}(CH_2SH)_2CH_2S\}(CO)_6]$; however, no such complex could be isolated. In every case, exclusively **7** was obtained in varying yields. The identity of **7** was established by elemental analysis (C, H, S), NMR spectroscopic studies ($^1$H, $^{13}$C, $^{29}$Si; solvent $CDCl_3$), mass-spectrometric investigations, IR spectroscopic studies, and crystal structure analysis (Figure 4; Supporting Information, Table S3).

As can be seen from Figure 4, each of the four iron coordination centers of **7** is surrounded by two bridging sulfur atoms, one iron atom, and three carbonyl groups. The four iron coordination polyhedra can be best described as strongly distorted octahedra, with three carbonyl groups in facial positions. All sulfur atoms of the tetradentate 4-fold deprotonated $Si(CH_2SH)_4$ ligand act as $\mu_2$-bridging atoms, leading to two bicyclic [2Fe2S] skeletons with a "butterfly" structure. The silicon atom

**Table 2.** Electrochemical Data for Compounds **5a**−**c** and **7** versus an $Ag/Ag^+$ Reference Electrode on a Carbon/Glassy Electrode

| compound | $E_{ox,1}$ [V] | $E_{red,1}$ [V] | $E_{red,2}$ [V] |
|---|---|---|---|
| **5a** | +0.79 | −1.48 ($E_{pc}$), −1.40 ($E_{pa}$) | |
| **5b** | +0.81 | −1.49 ($E_{pc}$), −1.40 ($E_{pa}$) | |
| **5c** | +0.81 | −1.49 ($E_{pc}$), −1.39 ($E_{pa}$) | |
| **7** | +0.99 | −1.05 ($E_{pc}$) irr. | −2.15 ($E_{pc}$), −1.89 ($E_{pa}$) |

is surrounded in a slightly distorted tetrahedral fashion. As already observed for **5a**−**c** and **6**, the Si−C−S angles (120.03(16)−121.88(16)°) differ significantly from the ideal tetrahedral angle.

**Electrochemical and Electrocatalytic Properties. Cyclic Voltammetry.** The electrocatalytic dihydrogen formation of [2Fe2S]-based model compounds for the [FeFe] hydrogenases has been well established.[5b,18] Therefore, it was of great interest to study also the electrochemical and related electrocatalytic properties of the model compounds **5a**−**c**, **6b**, and **7**.

The electrochemical behavior of these compounds in terms of their cyclic voltammograms is considered first. Analysis of **5a**−**c** shows the presence of an reversible anodic wave at around −1.48 V as expected for reduction of the diiron complexes.[19,20] The values obtained for the redox potentials recorded for **5a**−**c** are within the experimental error. This suggests that changes in the substituents on the silicon atom of these diiron complexes result in a minimal change of the electron density around the diiron centers and has negligible effect on the redox chemistry (Table 2). Since complexes **5a**−**c** exhibit similar electrochemical features, we focused our investigation on compound **5b**, and a detailed discussion of the electrochemical properties will be given representatively. The cyclic voltammetric reduction of **5b** in acetonitrile on a mercury dropping electrode (using tetraethylammonium perchlorate as the supporting electrolyte) is shown in Figure 5. The experimental cyclovoltammograms (CVs) are in good agreement with theoretical curves simulated on the basis of a two-electron reduction, where the second charge-transfer step is thermodynamically favored ($E°_2 > E°_1$) and kinetically faster ($k°_2 > k°_1$). CVs measured with slow scan rates ($< 5$ V $s^{-1}$) exhibit a distinct deviation from the ideal reversible behavior. It can be readily explained in terms of a slow irreversible follow-up reaction that occurs after the first reduction process, forming the decomposition product Q (reaction 4). The best fit between experimental and simulated CVs was obtained with the following parameter set:

$$\mathrm{Fe{-}Fe} + \mathrm{e^-} \rightleftharpoons \mathrm{Fe{-}Fe^-}$$
$$(E°_1 = -1.538\ \mathrm{V},\ \alpha_1 = 0.22,\ k°_1 = 0.4 \pm 0.1\ \mathrm{cm\ s^{-1}}) \quad (1)$$

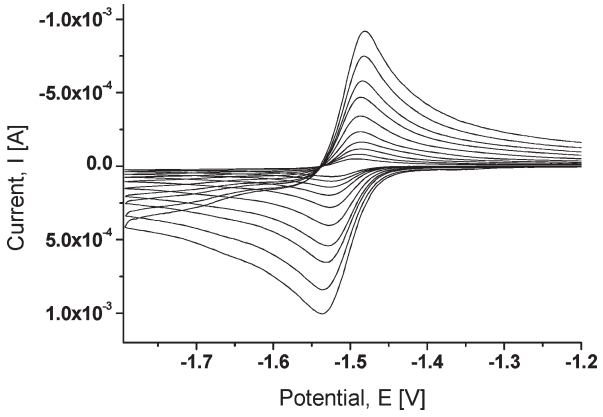


**Figure 5.** Cyclic voltammetric reduction of compound **5b** in acetonitrile (1.4 mM) on a mercury drop electrode using scan rates of 1, 3, 5, 10, 20, 40, 80, 120, 200, and 300 V $s^{-1}$.

$$\mathrm{Fe{-}Fe^-} + \mathrm{e^-} \rightleftharpoons \mathrm{{}^-Fe{-}Fe^-}$$
$$(E°_2 = -1.475\ \mathrm{V},\ \alpha_2 = 0.5,\ k°_2 \geq 1\ \mathrm{cm\ s^{-1}}) \quad (2)$$

$$\mathrm{{}^-Fe{-}Fe^-} + \mathrm{Fe{-}Fe} \rightleftharpoons \mathrm{Fe{-}Fe^-} + \mathrm{Fe{-}Fe^-}$$
$$(k_{f3} \approx 650\ \mathrm{L\ mol^{-1}\ s^{-1}}) \quad (3)$$

$$\mathrm{Fe{-}Fe^-} \rightarrow \mathrm{Q\ (decomposition)}$$
$$(k_{f4} \approx 50\ \mathrm{s^{-1}}) \quad (4)$$

It should be mentioned that the electrochemical reduction of **5b** is strongly dependent on the applied solvent-supporting electrolyte system. For instance, while $k°_2 > k°_1$ was found in acetonitrile/tetraethylammonium perchlorate, the reverse order $k°_1 > k°_2$ was observed when using tetra-*n*-butylammonium perchlorate. A much bigger difference in the electrochemical behavior (affecting even the qualitative appearance of the CVs) is observed when using *N*,*N*-dimethylformamide (DMF) instead of acetonitrile. The strong effect of the solvent and the supporting electrolyte can be readily explained via the stabilization of an in situ formed rotated state by the formation of a nitrile complex, which is not possible when using DMF (see also the section Reduction of **5b** with Sodium Amalgam and Quantum Chemical Calculations).

When compared with $[Fe_2\{\mu\text{-}SCH_2C(CH_3)_2CH_2S\}(CO)_6]$[21] and similar diiron complexes like $[Fe_2\{\mu\text{-}SCH_2XCH_2S\}(CO)_6]$ (X = $CR_2$, NR),[22] the $[Fe^IFe^I]$ state of the silicon-based analogues is easier to oxidize ($E_{ox,1}$) by about 100 mV; somewhat surprisingly, the reduction waves show that **5a**−**c** are also easier to reduce to the $[Fe^0Fe^0]$ level ($E_{red,1}$) by a similar amount, which is difficult to understand. The less positive oxidation potential would suggest that the electron density at the iron center has increased, but if this was the case, the reduction would be more difficult. The fact that this is not observed

(18) (a) Schwartz, L.; Eriksson, L.; Lomoth, R.; Teixidor, F.; Viñas, C.; Ott, S. *Dalton Trans*. **2008**, 2379–2381. (b) Yu, Z.; Wang, M.; Li, P.; Dong, W.; Wang, F.; Sun, L. *Dalton Trans*. **2008**, 2400–2406. (c) Ezzaher, S.; Orain, P.-Y.; Capon, J.-F.; Gloaguen, F.; Pétillon, F. Y.; Roisnel, T.; Schollhammer, P.; Talarmin, J. *Chem. Commun*. **2008**, 2547–2549. (d) Li, P.; Wang, M.; Pan, J.; Chen, L.; Wang, N.; Sun, L. *J. Inorg. Biochem*. **2008**, *102*, 952–959. (e) Song, L.-C.; Wang, H.-T.; Ge, J.-H.; Mei, S.-Z.; Gao, J.; Wang, L.-X.; Gai, B.; Zhao, L.-Q.; Yan, J.; Wang, Y.-Z. *Organometallics* **2008**, *27*, 1409–1416.

(19) Liu, T.; Wang, M.; Shi, Z.; Cui, H.; Dong, W.; Chen, J.; Åkermark, B.; Sun, L. *Chem.—Eur. J*. **2004**, *10*, 4474–4479.

(20) Apfel, U.-P.; Halpin, Y.; Görls, H.; Vos, J. G.; Schweizer, B.; Linti, G.; Weigand, W. *Chem. Biodiversity* **2007**, *4*, 2138–2148.

(21) Singleton, M. L.; Jenkins, R. M.; Klemashevich, C. L.; Darensbourg, M. Y. *C. R. Chim*. **2008**, *11*, 861–874.

(22) Felton, G. A. N.; Mebi, C. A.; Petro, B. J.; Vannucci, A. K.; Evans, D. H.; Glass, R. S.; Lichtenberger, D. L. *J. Organomet. Chem*. **2009**, *694*, 2681–2699, and references cited herein.

may suggest that the two redox processes involve different orbitals.

Where **5a**−**c** have one active site for the binding and production of dihydrogen, complex **7** has four iron centers bridged by an $Si(CH_2S\text{-}\mu)_4$ moiety and therefore contains two redox active sites. For this compound, one irreversible anodic wave is observed in the cyclic voltammetry representing the oxidation of the $Fe^I$ center to $Fe^{II}$ (see Figure 6). Although there are two diiron active sites in this complex, only one anodic wave is observed suggesting that the oxidation of each active site occurs simultaneously, and therefore this wave represents two one-electron processes.[5b] This result also indicates that there is little or no interaction across the $Si(CH_2S\text{-}\mu)_4$ bridge in the molecule.

This is again reflected by the presence of one irreversible reduction representing two one-electron processes corresponding to the $[Fe^IFe^I] + e^- \rightarrow [Fe^0Fe^I]$ process for each diiron center ($E_{red,1} = -1.05$ V). This is a positive shift of approximately 440 mV when compared to compounds **5a**−**c**.

The electrochemistry of the dinuclear complex **6b** is very different from that observed for the other species. The cyclic voltammogram and the differential pulse data in Figure 7 show reduction potentials at −1.38 and −1.57 V in the potential area for the commonly discussed $[Fe^IFe^I] + e^- \rightarrow [Fe^0Fe^I]$ reduction step in [2Fe2S] complexes.[20,23]

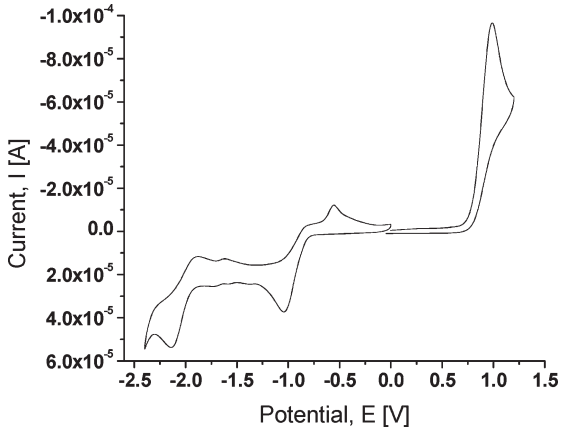


**Figure 6.** Cyclic voltammogram of compound **7** on a GC macro electrode, versus $Ag/Ag^+$, using 0.05 M $[n\text{-}Bu_4N][PF_6]$ in $CH_3CN$ as the supporting electrolyte.

A third reversible reduction is noted at more negative potentials ($E_{pc} = -2.16$ V). Compound **6b** shows two irreversible positive processes (see Figure 7), which might indicate an oxidation process as observed for **5a**−**c**. The presence of two separate anodic peaks may be due to the different coordination environment of the two metal centers and may also indicate electronic coupling across the dithiolato bridges between the two active sites as recently described by Surawatanawong et al.[24]

To allow comparison with the data reported by Pickett et al.,[16] the electrochemistry of compound **6b** has been carried out in dichloromethane, and the results obtained are shown in Table 3. The redox processes of these iron hydrogenase models are clearly solvent dependent, with negative shifts of approximately 100 mV observed when changing from dichloromethane to acetonitrile. An ill-defined oxidation is observed at a more positive potential than the corresponding process in acetonitrile. This wave is not associated with oxidation of the solvent since in blank electrolyte no such process is observed. The third reductive process detected in acetonitrile is not observed in dichloromethane because of solvent cutoff.

The first reduction wave of $[Fe_4\{\mu\text{-}MeC(CH_2S)_3\}_2(CO)_8]$ occurs at a potential that is approximately 140 mV more positive than that of the corresponding process in the related silicon compound $[Fe_4\{\mu\text{-}MeSi(CH_2S)_3\}_2(CO)_8]$ (**6b**). A difference of 100 mV is noted for the second reduction potential. However, comparison of the silicon-based hydrogenase analogue with the related carbon-based species would suggest that the presence of silicon does not greatly affect the reduction potentials. On the basis of the results obtained so far, we are not in the

**Table 3.** Electrochemical Data for Compound **6b** and the Related Carbon Compound $[Fe_4\{\mu\text{-}MeC(CH_2S)_3\}_2(CO)_8]$ in Acetonitrile and Dichloromethane[a]

| compound (solvent) | $E_{pa}$ [V] $Fe^IFe^{II}/Fe^{II}Fe^{II}$ | $E_{1/2}$ [V] $Fe^{II}Fe^I/Fe^IFe^I$ | $E_{1/2}$ [V] $Fe^IFe^I/Fe^0Fe^I$ |
|---|---|---|---|
| **6b** ($CH_3CN$) | +0.91 | −1.35 | −2.16 |
| | +1.04 | −1.52 | |
| **6b** ($CH_2Cl_2$) | +1.44 | −1.25 | |
| | | −1.43 | |
| $[Fe_4\{\mu\text{-}MeC(CH_2S)_3\}_2(CO)_8]$[16] ($CH_2Cl_2$) | | −1.11 | |
| | | −1.48 | |

[a] All values have been corrected against the $Ag/Ag^+$ reference electrode using the $Fc/Fc^+$ redox couple as an internal standard.

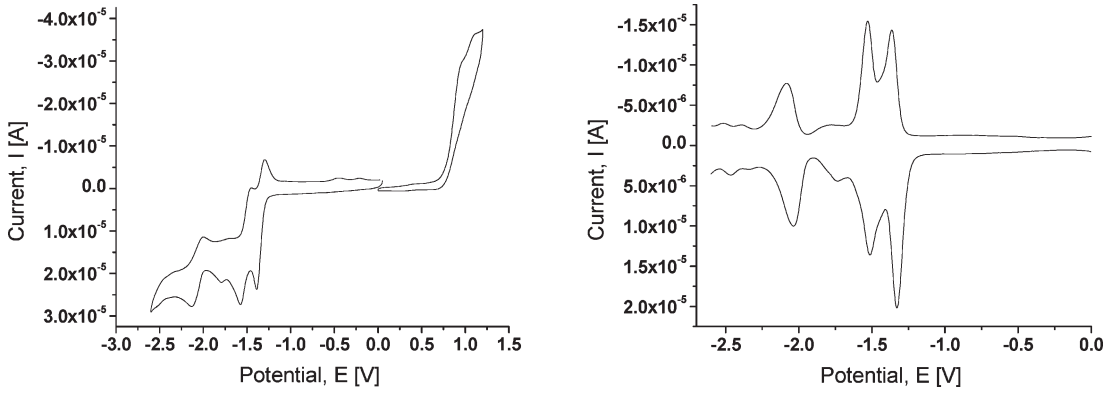


**Figure 7.** Cyclic voltammogram (left) and differential pulse voltammogram (right) of compound **6b** on a GC macro electrode, versus $Ag/Ag^+$, using 0.05 M $[n\text{-}Bu_4N][PF_6]$ in $CH_3CN$ as the supporting electrolyte.

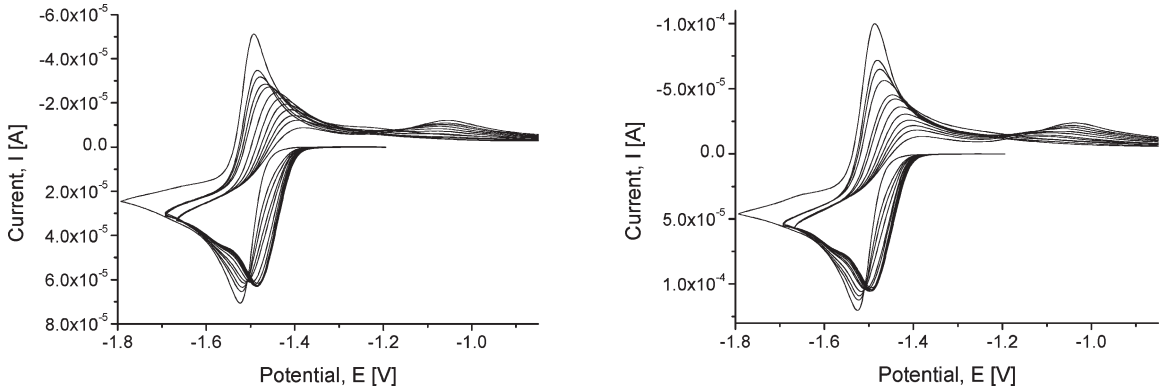


**Figure 8.** Cyclic voltammetric reduction of a 1.4 mM solution of **5b** in acetonitrile on a mercury drop electrode in the presence of varying concentrations of pivalic acid (right) and simulated CVs (left). The scan rate is 1 V $s^{-1}$. The HP concentration was varied as follows: [HP]/[**5b**] = 0 (leftmost CV), 1/3, 2/3, 1, 4/3, 5/3, 2, 8/3, 10/3, 4, 14/3, 16/3, and 20/3 (rightmost CV). Mechanism and simulation parameters are given by reactions 1 to 11.

position to assess the redox states of the iron centers in the silicon compound **6b** exactly, and further studies are underway to clarify this issue. However, compared to the carbon analogue described by Pickett et al., an [$Fe^{I}$-$Fe^{II}Fe^{II}Fe^{I}$] system can be assumed.

**Electrocatalysis.** To investigate the possible catalytic proton reduction of compounds **5a**−**c**, **6b**, and **7**, the electrochemistry of each complex was analyzed in the presence of a weak acid, acetic acid (AcOH) or pivalic acid (HP), in acetonitrile. In the case of compound **5b**, both acids (AcOH and HP) gave very similar results, and solely the results obtained with pivalic acid will be reported in the following.

The cyclic voltammetric reduction of **5b** in the presence of varying HP concentrations is shown in Figure 8 and Supporting Information, Figure S5.

Independently of the applied scan rate (1, 3, 5, and 10 V $s^{-1}$), the CVs are shifted on the potential scale in the positive direction, while the peak current is slightly decreased upon HP addition. Interestingly, a kind of "isosbestic point" is formed in the course of this. In analogy to UV−vis spectroscopy, such a behavior can be theoretically expected if there is an equilibrium between compound **5b** and another species formed upon HP addition, provided the CVs refer to the same scan rate and the kinetics of adjusting the equilibrium does not disturb the linear relationship between the current and the concentration within the time scale of the experiment. In view of the acid strength of HP in acetonitrile[25,26] and the relatively low HP concentrations used in our experiments, it is unlikely that a direct protonation of **5b** resulting in Fe−Fe−$H^+$ is responsible for the "isosbestic point". It is therefore more likely that an undissociated HP molecule is coordinated to the complex through hydrogen bonds, and the deprotonation of this HP molecule is initiated by the reduction of **5b** (either in the form of a concerted process or as a follow-up reaction). Indeed, a good agreement between experimental and simulated CVs (Figure 8; Supporting Information, Figure S5) was obtained by adding the following reactions to the eqs 1−4 (eqs 5, 10, and 11 cite refs 27, 28, and 29, respectively).

$$\mathrm{Fe{-}Fe} + \mathrm{HP} \rightleftharpoons \mathrm{Fe{-}Fe{-}HP} \quad (K_5 \approx 350 \pm 200,\ k_{f5} < 10^3\ \mathrm{L\ mol^{-1}\ s^{-1}})^{27} \qquad (5)$$

$$^{-}\mathrm{Fe{-}Fe^{-}} + \mathrm{HP} \rightleftharpoons {}^{-}\mathrm{Fe{-}Fe{-}HP}^{-} \quad (K_6/K_5 \approx 4,\ k_{f6} \approx 5 \times 10^8\ \mathrm{L\ mol^{-1}\ s^{-1}}) \qquad (6)$$

$$^{-}\mathrm{Fe{-}Fe{-}HP^{-}} + \mathrm{HP} \rightleftharpoons \mathrm{H{-}Fe{-}Fe{-}HP^{-}} + \mathrm{P^{-}} \quad (K_7 \leq 1, \text{diffusion controlled}) \qquad (7)$$

$$\mathrm{P^{-}} + \mathrm{HP} \rightleftharpoons \mathrm{HP{-}P^{-}} \quad (K_8 \geq 5000,\ k_{f8} > 2 \times 10^6\ \mathrm{L\ mol^{-1}\ s^{-1}}) \qquad (8)$$

$$\mathrm{Fe{-}Fe{-}HP} + \mathrm{e^{-}} \rightleftharpoons \mathrm{Fe{-}Fe{-}HP^{-}} \quad (E^{\circ}_3 = -1.48\ \mathrm{V},\ \alpha_3 = 0.55,\ k^{\circ}_3 \approx 0.4\ \mathrm{cm\ s^{-1}}) \qquad (9)$$

$$\mathrm{Fe{-}Fe{-}HP^{-}} + \mathrm{e^{-}} \rightarrow {}^{-}\mathrm{Fe{-}Fe{-}H} + \mathrm{P^{-}} \quad (E^{\circ}_4 = -1.168\mathrm{V},\ \alpha_4 = 0.45,\ k^{\circ}_4 = 1.75 \times 10^{-5}\ \mathrm{cm\ s^{-1}})^{28} \qquad (10)$$

(23) (a) Liu, Z.-P.; Hu, P. *J. Chem. Phys.* **2002**, *117*, 8177–8180. (b) Song, L.-C.; Gao, J.; Wang, H.-T.; Hua, Y.-J.; Fan, H.-T.; Zhang, X.-G.; Hu, Q.-M. *Organometallics* **2006**, *25*, 5724–5729. (c) Greco, C.; Zampella, G.; Bertini, L.; Bruschi, M.; Fantucci, P.; De Goia, L. *Inorg. Chem.* **2007**, *46*, 108–116. (d) Gao, W.; Ekström, J.; Liu, J.; Chen, C.; Eriksson, L.; Weng, L.; Åkermark, B.; Sun, L. *Inorg. Chem.* **2007**, *46*, 1981–1991.

(24) Surawatanawong, P.; Hall, M. B. *Inorg. Chem.* **2010**, *49*, 5737–5747.

(25) The p$K_a$ value of acetic acid in acetonitrile is 22.6 and that of pivalic acid should not be significantly different.

(26) Kosuke, I. *Acid-Base Dissociation Constants in Dipolar Aprotic Solvents*; Blackwell Scientific Publications: Oxford, 1990.

(27) The minimum of the standard deviation is only slightly depending on the exact value of $K_5$. There are several combinations of $K_6/K_5 \approx 4$ yielding virtually the same standard deviation between simulated and experimental CVs.

(28) Reaction 10 is fully irreversible. Consequently, there is an infinite number of $E^{\circ}/k^{\circ}$ combinations yielding exactly the same current curve. For this reason, the "right" combination cannot be determined exclusively from electrochemical data.

(29) Reaction 11 should be considered an overall reaction that occurs in several steps. It describes the re-oxidation of the species generated in reaction 10 and is necessary only to render the re-oxidation peak observed in the reverse scan at around −1.05 V.

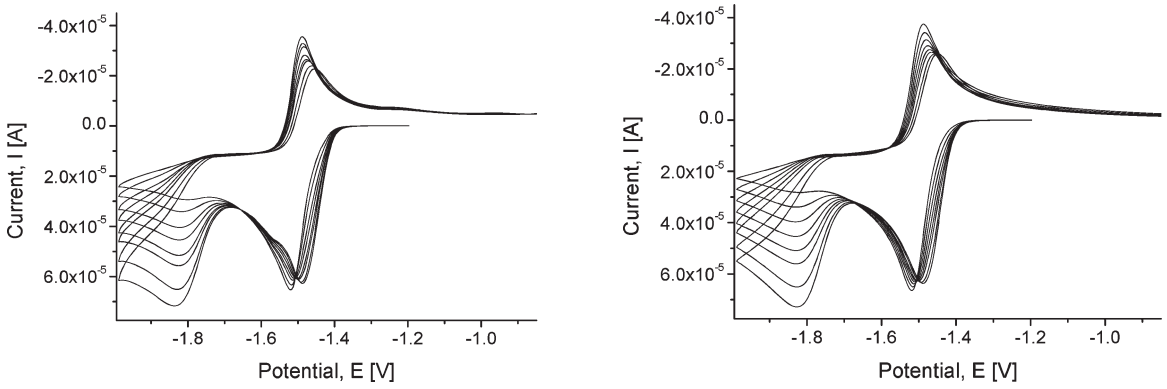


**Figure 9.** Cyclic voltammetric reduction of a 1.4 mM solution of **5b** in acetonitrile on a mercury drop electrode in the presence of varying concentrations of pivalic acid (left) and simulated CVs (right). The scan rate is 1 V $s^{-1}$. The HP concentration was varied as follows: [HP]/[**5b**] = 1/3, 2/3, 1, 4/3, 5/3, 2, 8/3, 10/3. The mechanism and simulation parameters are given by reactions 1−11.

$$\mathrm{Fe{-}Fe^- + HP + e^- \overset{P^-}{\leftarrow} {}^-Fe{-}Fe{-}H}$$
$$(E^\circ_5 = -1.168\ \mathrm{V},\ \alpha_5 = 0.6,\ k^\circ_5 = 0.1\ \mathrm{cm\ s^{-1}})^{29} \quad (11)$$

This mechanism also correctly reflects the experimental observation that the shift of the CVs in the positive direction upon HP addition converges to a constant value when reaching a ratio [HP]/[**5b**] of about 4:1. Any larger excess affects only the reverse (re-oxidation) scan of the CVs. It has virtually no effect on the forward (reduction) scan.[30]

As expected, no catalytic dihydrogen generation is observed in the presence of weak acids as long as two electrons are consumed by compound **5b** (around −1.5 V). However, a catalytic current is observed in the presence of pivalic (or acetic) acid if the electrode potential becomes more negative than about −1.8 V. Experimental CVs measured with a scan rate of 1 V $s^{-1}$ are shown in Figure 9. They are in excellent agreement with simulated ones (Figure 9).

The latter were obtained by adding the following reactions to the previous eqs 1−11:

$$\mathrm{H{-}Fe{-}Fe{-}HP^- + e^- \rightleftharpoons {}^-H - Fe{-}Fe{-}HP^-}$$
$$(E^\circ_6 = -1.77\ \mathrm{V},\ \alpha_6 = 0.5,\ k^\circ_6 \approx 0.2\ \mathrm{cm\ s^{-1}}) \quad (12)$$

$$\mathrm{{}^-H{-}Fe{-}Fe{-}HP^- \rightarrow Fe{-}Fe^- + P^- + H_2}$$
$$(k_{f13} = 7\ \mathrm{s^{-1}}) \quad (13)$$

$$\mathrm{{}^-H{-}Fe{-}Fe{-}HP^- + HP \rightarrow Fe{-}Fe{-}HP^- + P^- + H_2}$$
$$(k_{f14} = 2300\ \mathrm{L\ mol^{-1}\ s^{-1}}) \quad (14)$$

$$\mathrm{{}^-H{-}Fe{-}Fe{-}HP^- + HP \rightarrow H{-}Fe{-}Fe{-}HP^- + P^- + \frac{1}{2}H_2}$$
$$(k_{f15} = 13500\ \mathrm{L\ mol^{-1}\ s^{-1}}) \quad (15)$$

At least three catalytic reactions (reactions 13−15) must be taken into consideration to render the correct height and position of the cathodic current in the potential range at around −1.85 V as well as the correct shape and position of the re-oxidation peak at around −1.5 V as a function of the HP concentration. Figure 10 shows experimental CVs, which were measured on a mercury drop electrode.

Unlike the direct reduction of HP (which is thermodynamically possible but kinetically inhibited at the mercury drop electrode in the underlying potential range), the indirect reduction by homogeneous electron (reaction 15) becomes the dominating catalytic process for the 3-fold reduced complex. However, because of the second-order character of reaction 15, this statement holds true only for sufficiently high HP concentrations. At lower HP concentrations ([HP]/[**5b**] < 4:3), only the effect of reaction 13 is visible. Reaction 14 leads only to a marginal visible improvement but the standard deviation between simulated and experimental CVs becomes distinctly worse when disregarding this reaction. Finally, it must be mentioned that reactions 12−15 do not yet correctly describe some details observed on the short-time scale. Most noteworthy is the fact that the cathodic current in the potential range around −1.85 V is no longer peak shaped when using scan rates of several hundred volts per second. It converges to a plateau current. It is therefore more likely that the species initiating the catalytic cycle according to eq 12 is not the species H−Fe−Fe−$HP^-$ itself but rather a species formed in a preceding chemical reaction such as:

$$\mathrm{H{-}Fe{-}Fe{-}HP^- \rightleftharpoons H{-}Fe{-}Fe{-}H + P^-} \quad (16)$$

In other words, it might be necessary to formulate reactions 12−15 in terms of H−Fe−Fe−H instead of H−Fe−Fe−$HP^-$.

Upon addition of acid to a 1 mM solution of complex **7** in acetonitrile, shifts are noted for each of the reduction waves. The first of the cathodic peaks representing $[Fe^{I}Fe^{I}] + e^- \rightarrow [Fe^{0}Fe^{I}]$ exhibits a shift of approximately 160 mV in the negative direction, and the wave appears to

(30) It should be mentioned that this behavior is strongly dependent on the applied supporting electrolyte. It becomes even more pronounced when using tetra-*n*-butylammonium perchlorate instead of tetraethylammonium perchlorate. In that case, the "isosbestic point" is lost and a positive shift of less than 10 mV is observed virtually independently of the HP concentration unless the HP concentration becomes distinctly lower than [HP]/[**5b**] = 1.

split into two waves ($E_{pc}$ = −1.20 and −1.36 V) when the concentration of acid in solution is 1 mM. These two waves appear to merge again when the concentration of acid is 4 mM and above. The second reduction waves corresponding to the $[Fe^0Fe^I] + e^- \rightarrow [Fe^0Fe^0]$ process are shifted initially by approximately 200 mV to a more positive potential. This shift is decreasing with each increment of acid added. Both waves experience an increase in current intensity upon addition of 1 mM acid with this rise continuing for the second of these peaks as the concentration of acid increases (Figure 11).

The electrocatalytic properties toward dihydrogen formation of compound **6b** were also investigated. Upon addition of acid, the reduction potentials of the first two reduction peaks were shifted to more positive potentials by 15 and 120 mV for the first and second reduction processes, respectively. An increase in current intensity is observed with each sequential increment of acid added, suggesting dihydrogen formation catalyzed by the $[Fe^IFe^I]$ redox couple. As observed for compounds **5a**−**c**, large currents are found in the region of ∼ −1.8 V with increasing intensity for growing acid concentration suggesting an electrochemical catalytic process from the $[Fe^IFe^I]$ state (Figure 12).

**Tentative Mechanism.** The most striking results obtained in this study are the observation of an "isosbestic point", the formation of dihydrogen at three different potentials, and a shift in positive direction for the reduction potentials of compounds **5a**−**c** in the presence of acid. Similar anodic shifts have only been observed for functionalized diiron azadithiolates, interpreted in that case by protonation of the amino function. In the absence of a basic group for the compounds under consideration here, no currently proposed mechanism[5b,17,23] can explain the results obtained in this study. A possible alternative mechanism could be a "protonation" of the sulfur atom. However, to the best of our knowledge, no electrochemical and spectroscopic evidence for the protonation of coordinating sulfur in [FeFe] hydrogenase model systems has been reported. On the other hand, Glass et al. have shown on the basis of density functional theory (DFT) calculations and photoelectron spectroscopy that for related tin containing [2Fe2S] systems the $\sigma$(Sn−C) orbital interacts with a 3p(S) orbital.[10] These inductive and hyperconjugative interactions increase the electron density at the sulfur atom. As a direct result, the basicity of the thiolato sulfur atom increases. Taking into account the anodic shift observed for the compounds discussed in this contribution and the investigations of Glass et al.,[10] a new possible mechanism is proposed on the basis of eqs 1−15 (see Scheme 5), whereby $^-$Fe−Fe−H and $^-$Fe−Fe−HP$^-$ might be convertible under consideration of eq 16 (see also Supporting Information). Beside the aforementioned kinetic and thermodynamic characterization, four main aspects are visible from Scheme 5:

(i) The two electron reduction step in the absence of acid is accompanied by a structural rearrangement forming a rotated state.
(ii) In the presence of acid, an interaction between protons and the thiolato sulfur atoms is established.
(iii) The catalytically active species is generated by reduction of compounds **5a**−**c** (Fe−Fe$^-$ or $^-$Fe−Fe−HP).
(iv) Dihydrogen can be generated via three different pathways depending on the acid concentration.

To verify this catalytic mechanism, further experiments were performed that confirmed the presence of states **I** and **II** in the catalytic cycle shown in Scheme 5.

**Protonation of 5b with $HBF_4 \cdot Et_2O$.** To further prove the catalytic cycle and sulfur "protonation", compound

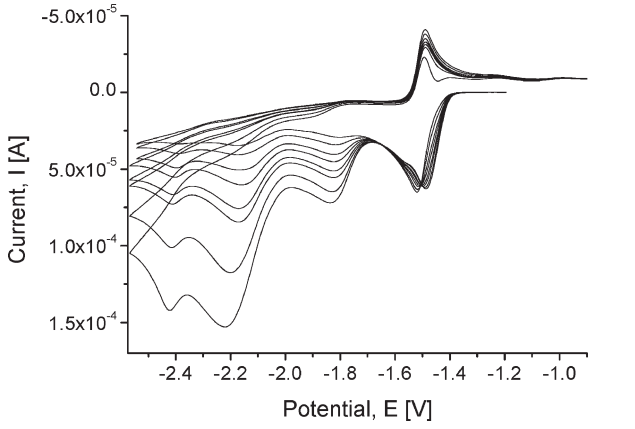


**Figure 10.** Cyclic voltammetric reduction of a 1.4 mM solution of **5b** in acetonitrile on a mercury drop electrode in the presence of varying concentrations of pivalic acid. The scan rate is 1 V $s^{-1}$. The HP concentration was varied as follows: [HP]/[**5b**] = 1/3, 2/3, 1, 4/3, 5/3, 2, 8/3, 10/3.

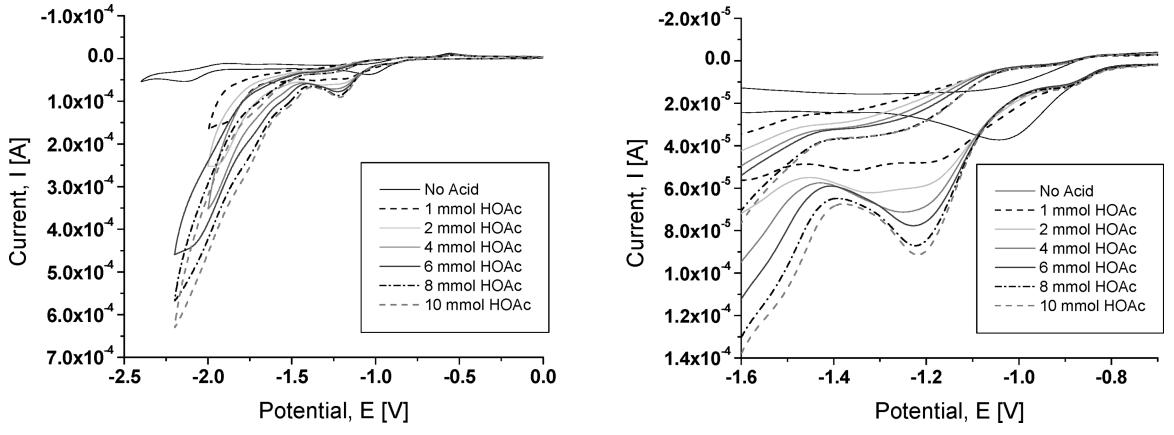


**Figure 11.** Cyclic voltammograms of compound **7** in acetonitrile (1 mM) in the presence of HOAc (0−10 mM), versus $Ag/Ag^+$.

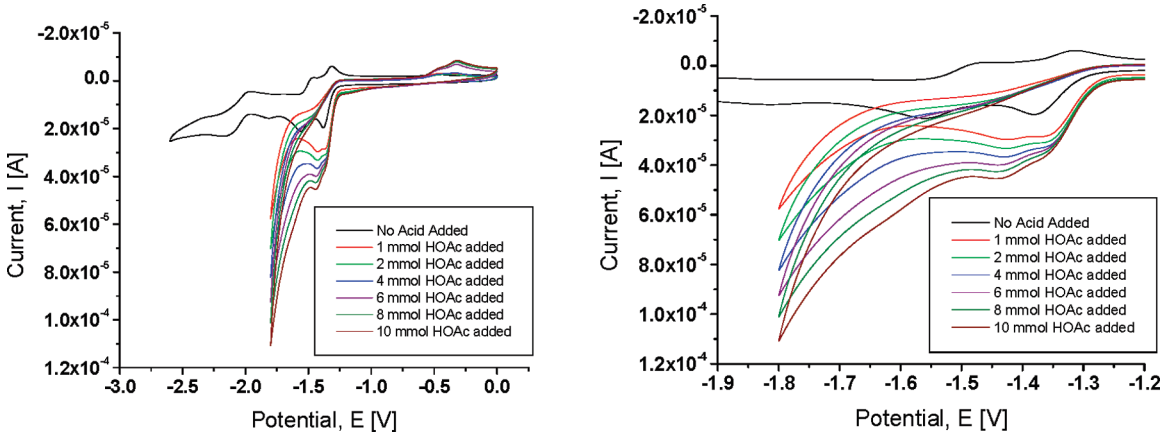


**Figure 12.** Cyclic voltammograms of compound **6b** in acetonitrile (1 mM) in the presence of HOAc (0−10 mM), versus $Ag/Ag^{+}$.

**Scheme 5.** Tentative Simplified Mechanism for the Dihydrogen Formation of the Silicon-Containing [FeFe] Hydrogenase Models **5a**−**c** According to Reaction Equations 1−15[a]

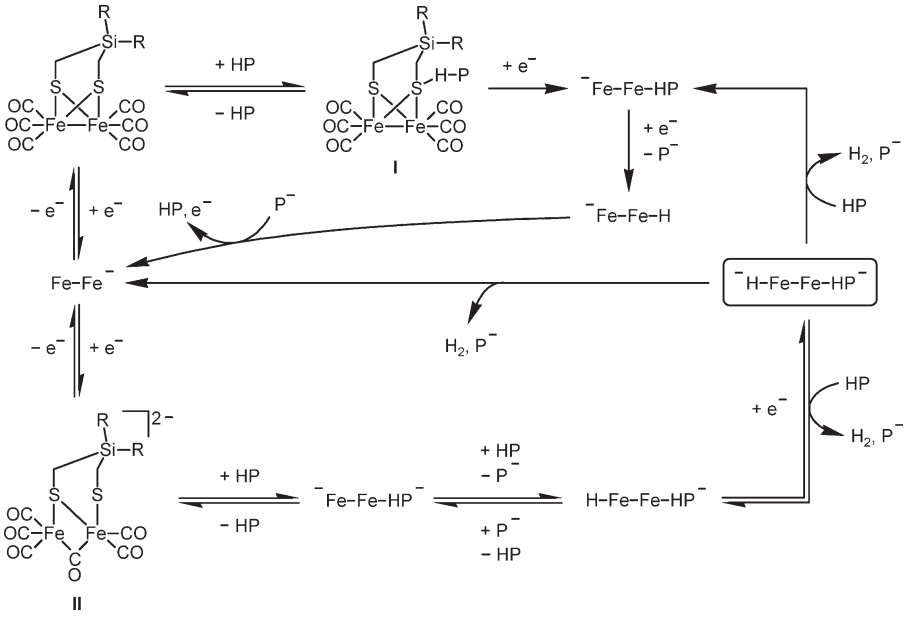


[a] For simplicity, the influence of eq 16 was neglected in this scheme.

**5b** was treated with tetrafluoroboric acid etherate ($HBF_4 \cdot Et_2O$); the resulting product was studied by IR spectroscopy. Figure 13 shows the difference between the IR spectra of **5b** before and after addition of $HBF_4 \cdot Et_2O$. Upon addition of $HBF_4 \cdot Et_2O$, a new absorption band at 2099 $cm^{-1}$ in the area of the C≡O vibrations is observed. This vibration suggests the existence of ligand protonated **5b**, as similar shifts were observed for [$Fe_2(\mu$-$SCH_2NHCH_2S)(CO)_6$] derivatives upon protonation.[31] $^1H$ NMR spectroscopic studies provided no signal at higher field (> −3 ppm) as reported for analogous $\mu$- or terminal-hydrides[32] and hint at a protonation at the sulfur atoms as depicted in Scheme 5. This, however, is in contrast to the calculations done by Darensbourg et al., who showed that protonation of the Fe−Fe bond pair should be favored opposed to the thiolato sulfur atoms.[7b]

**Reduction of 5b with Na/Hg and Quantum Chemical Calculations.** To elucidate the nature of the product formed in the two-electron reduction, compound **5b** was reacted with the strong reducing agent sodium amalgam in acetonitrile, whereupon the color of the solution changed to dark red. Figure 14 displays the experimental spectral properties of **5b** and the reduced species as well as the calculated IR bands.

In contrast to **5b**, the reduced species reveals an additional band at 1726 $cm^{-1}$ and hints at the formation of a bridging carbonyl ligand. To prove this assumption, quantum chemical calculations were performed. The experimental and calculated spectra of **5b** match very well (Figure 14). On this basis, the reduced species

(31) (a) Stanley, J. L.; Heiden, Z. M.; Rauchfuss, T. B.; Wilson, S. R.; De Gioia, L.; Zampella, G. *Organometallics* **2008**, *27*, 119–125. (b) Jiang, S.; Liu, J.; Shi, Y.; Wang, Z.; Åkermark, B.; Sun, L. *Dalton Trans.* **2007**, 896–902. (c) Xu, F.; Tard, C.; Wang, X.; Ibrahim, S. K.; Hughes, D. L.; Zhong, W.; Zeng, X.; Luo, Q.; Liu, X.; Pickett, C. J. *Chem. Commun.* **2008**, 606–608.

(32) (a) Barton, B. E.; Rauchfuss, T. B. *Inorg. Chem.* **2008**, *47*, 2261–2263. (b) Wang, N.; Wang, M.; Zhang, T.; Li, P.; Liu, J.; Sun, L. *Chem. Commun.* **2008**, 5800–5802.

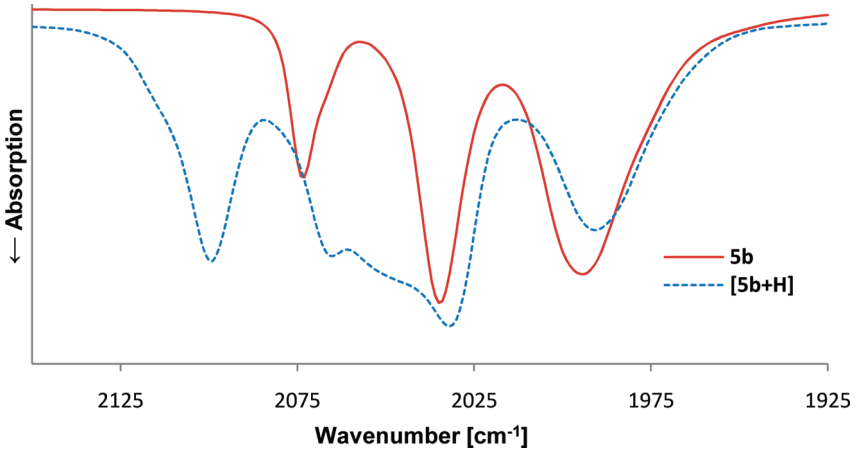


**Figure 13.** IR spectra of compound **5b** before (red) and after (blue) addition of $HBF_4 \cdot Et_2O$.

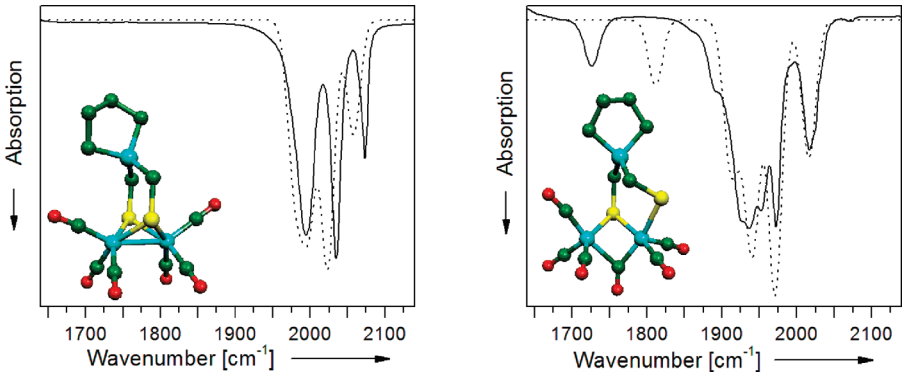


**Figure 14.** IR spectra (solid) and calculated IR spectra (dashed) of compound **5b** before (left) and after (right) addition of sodium amalgam.

$\mathbf{5b}^{2-}$ was also calculated. The best fit was obtained for the structure depicted in Figure 14, which is characterized by a broken sulfur−iron bond and a bridging CO ligand. The shift of the IR band (compared to the experimental IR band) of the bridging CO ligand to higher wavenumbers can be explained by the fact that these quantum chemical calculations were performed in the gas phase, and we have noticed that the solvent has a strong influence on the product formation: In contrast to the reduction in acetonitrile, reaction of **5b** with sodium amalgam in dichloromethane did not reveal any bridging CO band. We therefore assume that the resulting reduced complex is stabilized via a weak interaction with acetonitile. This assumption is further supported by calculations performed with an iron-bound acetonitrile molecule. In this case, a better agreement between theory and experiment was observed (Supporting Information, Figure S9); however, at higher wavenumbers the shape and the position of the CO bands strongly deviate.

## Conclusions

This study aimed at the investigation of the influence of sila-substitution (C/Si exchange) of carbon-based thiolato ligand systems of known [FeFe] hydrogenase models. For this purpose, the bis-, tris-, and tetrakis(mercaptomethyl)-silanes **4a**−**e** were synthesized and used as ligands for the synthesis of the iron complexes **5a**−**c**, **6a**, **6b**, and **7**. These compounds were characterized by elemental analyses (C, H, S), $^{1}H$, $^{13}C$, and $^{29}Si$ NMR spectroscopy, mass spectrometry, and single-crystal X-ray diffraction. The electrochemical behavior of the iron complexes was investigated via cyclic voltammetry, and the electrocatalytic properties for dihydrogen formation were studied. Sila-substitution was found to strongly affect the catalytic pathway. By introducing silicon, the basicity of the sulfur atoms increases, and this allows proton interaction with the thiolato sulfur atoms as observed by cyclic voltammetry and protonation experiments, coupled with IR studies. This finding is in contrast to the behavior of related complexes with carbon-based thiolato ligands; as shown by computational methods, for these compounds protonation of the Fe−Fe bond pair is favored.[7b] The redox features of **5a**−**c**, **6b**, and **7** are not straightforward. Introduction of silicon (C/Si exchange) seems to lead to compounds that are both easier to oxidize and to reduce. At this stage, this behavior is not fully understood. Compound **6b** has structural features similar to those reported by Pickett et al.[16] for the related carbon compound $[Fe_4\{\mu\text{-}MeC(CH_2S)_3\}_2(CO)_8]$. Addition of protons to compounds **5a**−**c** does not result in the formation of hydride complexes as observed by NMR spectroscopy, but IR studies do suggest protonation of sulfur. This observation is of great importance for the mechanism of the electrocatalytical dihydrogen formation proposed on the basis of electrochemical studies of **5b**. Furthermore, complex **5b** is, to the best of our knowledge, the only example leading to dihydrogen development at three different reduction potentials with high activity toward dihydrogen formation.

## Experimental Section

**General Procedures.** All syntheses were carried out under dry nitrogen or argon. The organic solvents used were dried and purified according to standard procedures and stored under dry

nitrogen or argon. Chemicals were used as received from Fluka or Acros without further purification. Thin layer chromatography (TLC): Merck silica gel 60 $F_{254}$ plates; detection under UV light at 254 nm. Flash chromatography (FC): Fluka silica gel 60. A Büchi GKR-51 apparatus was used for the bulb-to-bulb distillations. The $^{1}H$, $^{13}C\{^{1}H\}$, and $^{29}Si\{^{1}H\}$ NMR spectra were recorded at 23 °C on a Bruker DRX-300 NMR spectrometer ($^{1}H$, 300.1 MHz; $^{13}C$, 75.5 MHz; $^{29}Si$, 59.6 MHz). $CDCl_3$ or $CD_2Cl_2$ were used as the solvent. Chemical shifts (ppm) were determined relative to internal $CHCl_3$ ($^{1}H$, $\delta$ 7.24; $CDCl_3$), internal $CH_2Cl_2$ ($^{1}H$, $\delta$ 5.32; $CD_2Cl_2$), internal $CDCl_3$ ($^{13}C$, $\delta$ 77.0; $CDCl_3$), internal $CD_2Cl_2$ ($^{13}C$, $\delta$ 53.8; $CD_2Cl_2$), or external TMS ($^{29}Si$, $\delta$ 0; $CDCl_3$, $CD_2Cl_2$). Analysis and assignment of the $^{1}H$ NMR data were supported by $^{1}H,^{1}H$ COSY, $^{13}C,^{1}H$ HMQC, and $^{13}C,^{1}H$ HMBC experiments. Assignment of the $^{13}C$ NMR data was supported by DEPT 135, $^{13}C,^{1}H$ HMQC, and $^{13}C,^{1}H$ HMBC experiments. IR spectra were recorded on a Perkin-Elmer 2000 FT-IR spectrometer. A Jobin Yvon LabRam HR inverse spectrometer with a 632 nm HeNe-laser (Sacher Lasertechnik) was used for recording the Raman spectra. Mass-spectrometric studies (FAB/MS, DEI/MS) were performed on a SSQ710 Finnigan MAT spectrometer. Iron Mössbauer spectra were collected on a conventional constant acceleration spectrometer, with a source of $^{57}Co$ in Rh. The data were obtained at room temperature. Spectra were fitted to Lorentzian doublets using a standard least-squares minimization routine. The susceptibility measurements were made using a Quantum design SQUID magnetometer, in the range 4−300 K, with samples of mass approximately 10 mg mounted in gel caps in a plastic straw.

**Method A. Bis(chloromethyl)dimethylsilane (2a).** A 2.5 M solution of *n*-butyllithium in hexane (124 mL, 310 mmol of *n*-BuLi) was added dropwise at −70 °C (±3 °C, temperature measurement within the flask) within 5 h to a stirred mixture of dichlorodimethylsilane (**1a**) (20.0 g, 155 mmol), bromochloromethane (60.2 g, 465 mmol), and THF (190 mL) (the *n*-butyllithium solution was added via a special horizontally elongated side neck of the three-necked flask, which itself was immersed in the cooling bath to ensure precooling of the *n*-butyllithium solution before making contact with the reaction mixture). After the addition was complete, the mixture was stirred at −78 °C for 5 h and was then warmed to 20 °C within 17 h. The solvent was removed under reduced pressure (formation of a precipitate), and the residue was extracted with water (800 mL) and diethyl ether (800 mL). The organic extract was dried over anhydrous sodium sulfate, the solvent was removed under reduced pressure, and the residue was purified by bulb-to-bulb distillation (oven temperature 46 °C, 12 mbar) to give **2a** in 77% yield as a colorless liquid (18.8 g, 120 mmol). $^{1}H$ NMR ($CDCl_3$): $\delta$ 0.23 (s, 6 H, $SiCH_3$), 2.87 (s, 4 H, $SiCH_2Cl$). $^{13}C$ NMR ($CDCl_3$): $\delta$ −5.9 ($SiCH_3$), 28.1 ($SiCH_2Cl$). $^{29}Si$ NMR ($CDCl_3$): $\delta$ 3.9. Anal. Calcd for $C_4H_{10}Cl_2Si$: C, 30.58; H, 6.42. Found: C, 30.5; H, 6.5.

**Method B. Bis(acetylthiomethyl)dimethylsilane (3a).** Compound **2a** (5.00 g, 31.8 mmol) was added in a single portion at 20 °C to a stirred suspension of potassium thioacetate (10.9 g, 95.4 mmol) in THF (250 mL), and the resulting mixture was stirred at 20 °C for 21 h. The solvent was removed under reduced pressure, diethyl ether (300 mL) and water (200 mL) were added, the organic phase was separated, and the aqueous phase was extracted with diethyl ether (2 × 200 mL). All organic extracts were combined and dried over anhydrous sodium sulfate, the solvent was removed under reduced pressure, and the residue was purified by bulb-to-bulb distillation (oven temperature 95−100 °C, 0.5 mbar) to give **3a** in 86% yield as a yellowish liquid (6.44 g, 27.2 mmol). $^{1}H$ NMR ($CDCl_3$): $\delta$ 0.08 (s, 6 H, $SiCH_3$), 2.09 (s, 4 H, $SiCH_2S$), 2.28 (s, 6 H, $C(O)CH_3$). $^{13}C$ NMR ($CDCl_3$): $\delta$ −3.8 ($SiCH_3$), 12.3 ($SiCH_2S$), 30.0 ($C(O)CH_3$), 196.0 ($C(O)CH_3$). $^{29}Si$ NMR ($CDCl_3$): $\delta$ 3.4. Anal. Calcd for $C_8H_{16}O_2S_2Si$: C, 40.64; H, 6.82; S, 27.12. Found: C, 40.3; H, 6.6; S, 26.5.

**Method C. Bis(mercaptomethyl)dimethylsilane (4a).** A solution of **3a** (6.04 g, 25.5 mmol) in diethyl ether (90 mL) was added dropwise at 0 °C within 2 h to a stirred suspension of lithium aluminum hydride (4.91 g, 129 mmol) in diethyl ether (150 mL), and the resulting mixture was stirred at 0 °C for a 90 min and then at 20 °C for a further 19 h. Subsequently, hydrochloric acid (2 M, 50 mL) was added dropwise with stirring at 0 °C within 30 min, and the resulting mixture was then warmed to 20 °C, followed by the addition of water (100 mL). The organic phase was separated, the aqueous phase was extracted with diethyl ether (2 × 200 mL), the combined organic extracts were dried over anhydrous sodium sulfate, the solvent was removed under reduced pressure, and the residue was purified by bulb-to-bulb distillation (oven temperature 40−45 °C, 0.2 mbar) to give **4a** in 80% yield as a colorless liquid (3.13 g, 20.5 mmol). $^{1}H$ NMR ($CDCl_3$): $\delta$ 0.15 (s, 6 H, $SiCH_3$), 1.16 (t, $^{3}J_{HH}$ = 7.2 Hz, 2 H, SH), 1.72 (d, $^{3}J_{HH}$ = 7.2 Hz, 4 H, $SiCH_2S$). $^{13}C$ NMR ($CDCl_3$): $\delta$ −4.9 ($SiCH_3$), 5.9 ($SiCH_2S$). $^{29}Si$ NMR ($CDCl_3$): $\delta$ 5.1. Anal. Calcd for $C_4H_{12}S_2Si$: C, 31.53; H, 7.94; S, 42.09. Found: C, 31.4; H, 7.6; S, 41.3.

**1,1-Bis(chloromethyl)-1-silacyclopentane (2b).** This compound was synthesized according to Method A from 1,1-dichloro-1-silacyclopentane (**1b**) (25.0 g, 161 mmol), bromochloromethane (62.7 g, 485 mmol), a 2.5 M solution of *n*-butyllithium in hexanes (129 mL, 323 mmol of *n*-BuLi), and THF (170 mL) to give **2b** in 61% yield as a colorless liquid (18.0 g, 98.3 mmol); bp 83−86 °C/8 mbar. $^{1}H$ NMR ($CDCl_3$): $\delta$ 0.76−0.81 (m, 4 H, $SiCH_2C$), 1.63−1.68 (m, 4 H, $SiCH_2CH_2C$), 2.97 (s, 4 H, $SiCH_2Cl$). $^{13}C$ NMR ($CDCl_3$): $\delta$ 8.7 ($SiCH_2C$), 26.6 ($SiCH_2Cl$), 26.9 ($SiCH_2CH_2C$). $^{29}Si$ NMR ($CDCl_3$): $\delta$ 20.9. Anal. Calcd for $C_6H_{12}Cl_2Si$: C, 39.35; H, 6.60. Found: C, 39.3; H, 6.7.

**1,1-Bis(acetylthiomethyl)-1-silacyclopentane (3b).** This compound was synthesized according to Method B from **2b** (4.00 g, 21.8 mmol), potassium thioacetate (7.48 g, 65.5 mmol), and THF (150 mL) to give **3b** in 77% yield as a yellowish liquid (4.40 g, 16.8 mmol); bp 130 °C/0.2 mbar. $^{1}H$ NMR ($CDCl_3$): $\delta$ 0.60−0.65 (m, 4 H, $SiCH_2C$), 1.54−1.59 (m, 4 H, $SiCH_2CH_2C$), 2.19 (s, 4 H, $SiCH_2S$), 2.30 (s, 6 H, $C(O)CH_3$). $^{13}C$ NMR ($CDCl_3$): $\delta$ 10.4 ($SiCH_2S$), 11.1 ($SiCH_2C$), 27.0 ($SiCH_2CH_2C$), 30.0 ($C(O)CH_3$), 196.1 ($C(O)CH_3$). $^{29}Si$ NMR ($CDCl_3$): $\delta$ 19.6. Anal. Calcd for $C_{10}H_{18}O_2S_2Si$: C, 45.76; H, 6.91; S, 24.43. Found: C, 46.2; H, 6.8; S, 23.9.

**1,1-Bis(mercaptomethyl)-1-silacyclopentane (4b).** This compound was synthesized according to Method C from **3b** (4.27 g, 16.3 mmol), lithium aluminum hydride (4.00 g, 105 mmol), and diethyl ether (170 mL) to give **4b** in 67% yield as a colorless liquid (1.95 g, 10.9 mmol); bp 80−90 °C/0.1 mbar. $^{1}H$ NMR ($CDCl_3$): $\delta$ 0.67−0.72 (m, 4 H, $SiCH_2C$), 1.20 (t, $^{3}J_{HH}$ = 7.2 Hz, 2 H, SH), 1.58−1.63 (m, 4 H, $SiCH_2CH_2C$), 1.81 (d, $^{3}J_{HH}$ = 7.2 Hz, 4 H, $SiCH_2S$). $^{13}C$ NMR ($CDCl_3$): $\delta$ 4.3 ($SiCH_2S$), 9.4 ($SiCH_2C$), 27.1 ($SiCH_2CH_2C$). $^{29}Si$ NMR ($CDCl_3$): $\delta$ 22.7. Anal. Calcd for $C_6H_{14}S_2Si$: C, 40.40; H, 7.91; S, 35.95. Found: C, 40.5; H, 7.7; S, 35.2.

**1,1-Bis(chloromethyl)-1-silacyclohexane (2c).** This compound was synthesized according to Method A from 1,1-dichloro-1-silacyclohexane (**1c**) (27.0 g, 160 mmol), bromochloromethane (62.0 g, 479 mmol), a 2.5 M solution of *n*-butyllithium in hexanes (128 mL, 320 mmol of *n*-BuLi), and THF (185 mL) to give **2c** in 37% yield as a colorless liquid (11.8 g, 59.8 mmol); bp 112−114 °C/15 mbar. $^{1}H$ NMR ($CDCl_3$): $\delta$ 0.82−0.86 (m, 4 H, $SiCH_2C$), 1.39−1.46 (m, 2 H, $Si(CH_2)_2CH_2C$), 1.65−1.73 (m, 4 H, $SiCH_2CH_2C$), 2.95 (s, 4 H, $SiCH_2Cl$). $^{13}C$ NMR ($CDCl_3$): $\delta$ 8.5 ($SiCH_2C$), 24.0 ($SiCH_2CH_2C$), 26.1 ($SiCH_2Cl$), 29.3 ($Si(CH_2)_2CH_2C$). $^{29}Si$ NMR ($CDCl_3$): $\delta$ −1.3. Anal. Calcd for $C_7H_{14}Cl_2Si$: C, 42.64; H, 7.16. Found: C, 42.6; H, 7.1.

**1,1-Bis(acetylthiomethyl)-1-silacyclohexane (3c).** This compound was synthesized according to Method B from **2c** (3.98 g, 20.2 mmol), potassium thioacetate (6.95 g, 60.9 mmol), and THF (150 mL) to give **3c** in 91% yield as a yellowish liquid (5.09 g, 18.4 mmol); bp 130−140 °C/0.3 mbar. $^{1}H$ NMR ($CDCl_3$): $\delta$ 0.64−0.69

(m, 4 H, SiC$H_2$C), 1.30−1.38 (m, 2 H, Si(CH$_2$)$_2$C$H_2$C), 1.58−1.66 (m, 4 H, SiCH$_2$C$H_2$C), 2.14 (s, 4 H, SiC$H_2$S), 2.28 (s, 6 H, C(O)C$H_3$). $^{13}$C NMR ($CDCl_3$): $\delta$ 10.1 (Si$CH_2$S), 10.6 (Si$CH_2$C), 23.9 (SiCH$_2$$CH_2$C), 29.3 (Si(CH$_2$)$_2$$CH_2$C), 30.0 (C(O)$CH_3$), 196.1 ($C$(O)CH$_3$). $^{29}$Si NMR ($CDCl_3$): $\delta$ −1.6. Anal. Calcd for $C_{11}H_{20}O_2S_2Si$: C, 47.78; H, 7.29; S, 23.19. Found: C, 47.6; H, 7.1; S, 23.1.

**1,1-Bis(mercaptomethyl)-1-silacyclohexane (4c).** This compound was synthesized according to Method C from **3c** (2.47 g, 8.93 mmol), lithium aluminum hydride (2.19 g, 57.7 mmol), and diethyl ether (85 mL) to give **4c** in 69% yield as a colorless liquid (1.19 g, 6.18 mmol); bp 95 °C/0.2 mbar. $^1$H NMR ($CDCl_3$): $\delta$ 0.73−0.78 (m, 4 H, SiC$H_2$C), 1.21 (t, $^3J_{HH}$ = 7.1 Hz, 2 H, S$H$), 1.35−1.43 (m, 2 H, Si(CH$_2$)$_2$C$H_2$C), 1.61−1.69 (m, 4 H, SiCH$_2$C$H_2$C), 1.80 (d, $^3J_{HH}$ = 7.1 Hz, 4 H, SiC$H_2$S). $^{13}$C NMR ($CDCl_3$): $\delta$ 3.3 (Si$CH_2$S), 9.6 (Si$CH_2$C), 24.2 (SiCH$_2$$CH_2$C), 29.5 (Si(CH$_2$)$_2$$CH_2$C). $^{29}$Si NMR ($CDCl_3$): $\delta$ 0.2. Anal. Calcd for $C_7H_{16}S_2Si$: C, 43.69; H, 8.38; S, 33.33. Found: C, 43.7; H, 8.3; S, 33.0.

**Tris(chloromethyl)methylsilane (2d).** This compound was synthesized according to Method A from trichloro(methyl)silane (**1d**) (13.5 g, 90.3 mmol), bromochloromethane (52.9 g, 409 mmol), a 2.5 M solution of *n*-butyllithium in hexanes (110 mL, 275 mmol of *n*-BuLi), and THF (150 mL) to give **2d** in 72% yield as a colorless liquid (12.5 g, 65.3 mmol); bp 65 °C/0.4 mbar. $^1$H NMR ($CDCl_3$): $\delta$ 0.37 (s, 3 H, SiC$H_3$), 3.01 (s, 6 H, SiC$H_2$Cl). $^{13}$C NMR ($CDCl_3$): $\delta$ −8.6 (Si$CH_3$), 25.3 (Si$CH_2$Cl). $^{29}$Si NMR ($CDCl_3$): $\delta$ 2.5. Anal. Calcd for $C_4H_9Cl_3Si$: C, 25.08; H, 4.74. Found: C, 25.3; H, 4.8.

**Tris(acetylthiomethyl)methylsilane (3d).** This compound was synthesized according to Method B from **2d** (5.76 g, 30.1 mmol), potassium thioacetate (15.5 g, 136 mmol), and THF (400 mL) to give **3d** in 92% yield as a yellowish liquid (8.57 g, 27.6 mmol); bp 140−150 °C/0.1 mbar. $^1$H NMR ($CDCl_3$): $\delta$ 0.16 (s, 3 H, SiC$H_3$), 2.18 (s, 6 H, SiC$H_2$S), 2.31 (s, 9 H, C(O)C$H_3$). $^{13}$C NMR ($CDCl_3$): $\delta$ −5.4 (Si$CH_3$), 10.8 (Si$CH_2$S), 30.1 (C(O)$CH_3$), 195.6 ($C$(O)CH$_3$). $^{29}$Si NMR ($CDCl_3$): $\delta$ 3.4. Anal. Calcd for $C_{10}H_{18}O_3S_3Si$: C, 38.68; H, 5.84; S, 30.98. Found: C, 38.7; H, 5.8; S, 30.9.

**Tris(mercaptomethyl)methylsilane (4d).** This compound was synthesized according to Method C from **3d** (8.57 g, 27.6 mmol), lithium aluminum hydride (7.80 g, 206 mmol), and diethyl ether (350 mL) to give **4d** in 92% yield as a colorless liquid (4.69 g, 25.4 mmol); bp 80−90 °C/0.1 mbar. $^1$H NMR ($CDCl_3$): $\delta$ 0.25 (s, 3 H, SiC$H_3$), 1.27 (t, $^3J_{HH}$ = 7.4 Hz, 3 H, S$H$), 1.84 (d, $^3J_{HH}$ = 7.4 Hz, 6 H, SiC$H_2$S). $^{13}$C NMR ($CDCl_3$): $\delta$ −7.1 (Si$CH_3$), 3.8 (Si$CH_2$S). $^{29}$Si NMR ($CDCl_3$): $\delta$ 5.1. Anal. Calcd for $C_4H_{12}S_3Si$: C, 26.05; H, 6.56; S, 52.16. Found: C, 26.0; H, 6.4; S, 51.5.

**Tetrakis(mercaptomethyl)silane (4e).** This compound was synthesized according to ref 14a.

**Method D. General Procedure for the Synthesis of the Iron Complexes.** The respective (mercaptomethyl)silane (50 mg) and 0.5 mol equiv of $Fe_3(CO)_{12}$ per SH group were dissolved in toluene (30 mL). The resulting solution was heated under reflux for 2 h, the solvent was removed under reduced pressure, and the residue was purified via FC (eluent, THF/*n*-hexane (1:6 (v/v)); detection of the relevant fractions via TLC) to afford the respective iron complexes **5a**−**c**, **6a**, **6b**, and **7** as red crystalline solids.

**Diiron Complex 5a.** This compound was prepared according to Method D by treatment of **4a** (50 mg, 328 $\mu$mol) with $Fe_3(CO)_{12}$ (166 mg, 330 $\mu$mol) to afford **5a** (81 mg, 188 $\mu$mol) in 57% yield. $^1$H NMR ($CDCl_3$): $\delta$ 0.09 (s, 6 H, SiC$H_3$), 1.44 (s, 4 H, SiC$H_2$S). $^{13}$C NMR ($CDCl_3$): $\delta$ −0.3 (Si$CH_3$), 5.9 (Si$CH_2$S), 207.5 ($CO$). $^{29}$Si NMR ($CDCl_3$): $\delta$ 0.3. MS (DEI): $m/z$, 430 [M]$^+$, 402 [M − CO]$^+$, 374 [M − 2CO]$^+$, 346 [M − 3CO]$^+$, 318 [M − 4CO]$^+$, 290 [M − 5CO]$^+$, 262 [M − 6CO]$^+$. IR (KBr): 2074 (vs), 2031 (vs), 1987 (vs), 1949 (s), 1935 (s). Anal. Calcd for $C_{10}H_{10}Fe_2O_6S_2Si$: C, 27.93; H, 2.34; S, 14.91. Found: C, 28.5; H, 2.6, S; 14.4.

**Diiron Complex 5b.** This compound was prepared according to Method D by treatment of **4b** (50 mg, 280 $\mu$mol) with $Fe_3(CO)_{12}$ (142 mg, 282 $\mu$mol) to afford **5b** (116 mg, 250 $\mu$mol) in 89% yield (related to **5b**·0.1THF). $^1$H NMR ($CDCl_3$): $\delta$ 0.61−0.65 (m, 4 H, SiC$H_2$C), 1.45−1.55 (m, 8 H, SiC$H_2$S and SiCH$_2$C$H_2$C). $^{13}$C NMR ($CDCl_3$): $\delta$ 5.9 (Si$CH_2$S), 13.2 (Si$CH_2$C), 26.5 (SiCH$_2$$CH_2$C), 207.3 ($CO$). $^{29}$Si NMR ($CDCl_3$): $\delta$ 19.3. MS (DEI): $m/z$, 456 [M]$^+$, 428 [M − CO]$^+$, 400 [M − 2CO]$^+$, 372 [M − 3CO]$^+$, 344 [M − 4CO]$^+$, 316 [M − 5CO]$^+$, 288 [M − 6CO]$^+$. IR (KBr): 2070 (vs), 2028 (vs), 2004 (vs), 1971 (vs), 1956 (vs). Anal. Calcd for $C_{12}H_{12}Fe_2O_6S_2Si$·0.1THF: C, 32.14; H, 2.78; S, 13.84. Found: C, 32.2; H, 3.1; S, 14.2.

**Diiron Complex 5c.** This compound was synthesized according to Method D by treatment of **4c** (50 mg, 260 $\mu$mol) with $Fe_3(CO)_{12}$ (131 mg, 260 $\mu$mol) to afford **5c** (84 mg, 173 $\mu$mol) in 67% yield (related to **5c**·0.2THF). $^1$H NMR ($CDCl_3$): $\delta$ 0.63−0.68 (m, 4 H, SiC$H_2$C), 1.28−1.60 (m, 10 H, Si$CH_2$S, SiCH$_2$C$H_2$C, and Si(CH$_2$)$_2$C$H_2$C). $^{13}$C NMR ($CDCl_3$): $\delta$ 3.9 (Si$CH_2$S), 13.4 (Si$CH_2$C), 23.8 (SiCH$_2$$CH_2$C), 29.2 (Si(CH$_2$)$_2$$CH_2$C), 207.5 ($CO$). $^{29}$Si NMR ($CDCl_3$): $\delta$ −4.5. MS (DEI): $m/z$, 470 [M]$^+$, 442 [M − CO]$^+$, 414 [M − 2CO]$^+$, 386 [M − 3CO]$^+$, 358 [M − 4CO]$^+$, 330 [M − 5CO]$^+$, 302 [M − 6CO]$^+$. IR (KBr): 2914 (s), 2854 (m), 2070 (vs), 2017 (vs, b), 1637 (m), 1445 (m). Anal. Calcd for $C_{13}H_{14}Fe_2O_6S_2Si$·0.2THF: C, 34.21; H, 3.24, S; 13.23. Found: C, 34.2; H, 3.2; S, 13.5.

**Diiron Complex 6a and Tetrairon Complex 6b.** These compounds were synthesized according to Method D (except for the stoichiometric ratio) by treatment of **4d** (300 mg, 1.63 mmol) with $Fe_3(CO)_{12}$ (819 mg, 1.63 mmol) to afford two products, the orange-colored compound **6a** (isolated as **6a**·0.2hexane; 58 mg, 121 $\mu$mol) in 7% yield and the dark red compound **6b** (isolated as **6b**·1.3hexane; 132 mg, 143 $\mu$mol) in 9% yield.

**Compound 6a.** $^1$H NMR ($CDCl_3$): $\delta$ 0.22 and 0.31 (2 s, 6 H, SiC$H_3$), 0.98−1.14 (m, 1 H, SH), 1.37−1.79 (m, 6 H, SiC$H_2$S). $^{13}$C NMR ($CDCl_3$): $\delta$ −2.5 (Si$CH_3$), 4.1 and 9.0 (Si$CH_2$S), 207.1 ($CO$). MS (FAB, in nba): $m/z$, 464 [M + 2H]$^+$, 436 [M + 2H − CO]$^+$, 408 [M + 2H − 2CO]$^+$, 380 [M + 2H − 3CO]$^+$, 352 [M + 2H − 4CO]$^+$. IR (KBr): 2960 (m), 2925 (m), 2853 (m), 2073 (vs), 2032 (vs), 1995 (vs). Raman: 2593 cm$^{-1}$ ($\nu_{S-H}$). Anal. Calcd for $C_{10}H_{10}Fe_2O_6S_3Si$·0.2hexane: C, 28.1; H, 2.7, S; 20.1. Found: C, 28.1; H, 2.7; S, 15.2. Although the analytical data for "S" are unsatisfactory, the results of the FAB-MS studies and the NMR, IR, and Raman data are consistent with the formula $C_{10}H_{10}Fe_2O_6S_3Si$.

**Compound 6b.** $^1$H NMR ($CD_2Cl_2$): $\delta$ 0.05 (s, 6 H, SiC$H_3$), 0.52 (d, $^2J_{HH}$ = 14.8 Hz, 2 H, SiC$H_2$S-a), 0.86 (d, $^2J_{HH}$ = 14.8 Hz, 2 H, SiC$H_2$S-a), 1.55 (d, $^2J_{HH}$ = 14.4 Hz, 2 H, SiC$H_2$S-b), 1.83 (d, $^2J_{HH}$ = 14.4 Hz, 2 H, SiC$H_2$S-c), 2.24 (d, $^2J_{HH}$ = 14.4 Hz, 2 H, SiC$H_2$S-b), 3.20 (d, $^2J_{HH}$ = 14.4 Hz, 2 H, SiC$H_2$S-c). $^{13}$C NMR ($CD_2Cl_2$): $\delta$ −1.6 (Si$CH_3$), 5.6 (Si$CH_2$S-a), 9.9 (Si$CH_2$S-b), 21.4 (Si$CH_2$S-c), 208.0 and 208.8 ($CO$). MS (FAB, in nba): $m/z$, 810 [M]$^+$, 782 [M − CO]$^+$, 754 [M − 2CO]$^+$, 726 [M − 3CO]$^+$, 698 [M − 4CO]$^+$, 670 [M − 5CO]$^+$, 642 [M − 6CO]$^+$, 614 [M − 7CO]$^+$, 586 [M − 8CO]$^+$. IR (KBr): 2922 (m), 2854 (m), 2071 (m), 2038 (vs), 1982 (vs), 1943 (m). Anal. Calcd for $C_{16}H_{18}Fe_4O_8S_6Si_2$·1.3hexane: C, 31.0; H, 4.0, S; 20.9. Found: C, 30.9; H, 4.1; S, 20.6.

**Tetrairon Complex 7.** This compound was synthesized according to Method D by treatment of **4e** (50 mg, 231 $\mu$mol) with $Fe_3(CO)_{12}$ (233 mg, 463 $\mu$mol) to afford **7** (72 mg, 93.3 $\mu$mol) in 40% yield. $^1$H NMR ($CDCl_3$): $\delta$ 1.51 (s, 8 H, SiC$H_2$S). $^{13}$C NMR ($CDCl_3$): $\delta$ 5.3 (Si$CH_2$S), 206.8 ($CO$). $^{29}$Si NMR ($CDCl_3$): $\delta$ −6.4. MS (DEI): $m/z$, 772 [M]$^+$, 744 [M − CO]$^+$, 716 [M − 2CO]$^+$, 688 [M − 3CO]$^+$, 660 [M − 4CO]$^+$, 632 [M − 5CO]$^+$, 604 [M − 6CO]$^+$, 576 [M − 7CO]$^+$, 548 [M − 8CO]$^+$, 520 [M − 9CO]$^+$, 492 [M − 10CO]$^+$, 464 [M − 11CO]$^+$, 436 [M − 12CO]$^+$. IR (KBr): 2925 (s), 2854 (m), 2072 (vs), 2034 (vs), 2012 (vs), 1630 (m). Anal. Calcd for $C_{16}H_8Fe_4O_{12}S_4Si$: C, 24.89; H, 1.04; S, 16.62. Found: C, 25.1; H, 1.0; S, 16.5.

**Table 4.** Crystal Data and Refinement Details for the Crystal Structure Analyses of Compounds **5a**−**c**, **6b**, and **7**

| | **5a** | **5b** | **5c** | **6b** | **7** |
|---|---|---|---|---|---|
| empirical formula | $C_{10}H_{10}Fe_2O_6S_2Si$ | $C_{12}H_{12}Fe_2O_6S_2Si$ | $C_{13}H_{14}Fe_2O_6S_2Si$ | $C_{16}H_{18}Fe_4O_8S_6Si_2$ | $C_{16}H_8Fe_4O_{12}S_4Si$ |
| formula mass [g·mol$^{-1}$] | 430.09 | 456.13 | 470.15 | 810.24 | 771.95 |
| collection $T$ [°C] | −90(2) | −90(2) | −90(2) | −90(2) | −90(2) |
| $\lambda$ (Mo K$_\alpha$) [Å] | 0.71073 | 0.71073 | 0.71073 | 0.71073 | 0.71073 |
| crystal system | monoclinic | monoclinic | triclinic | triclinic | triclinic |
| space group (No.) | $P2_1/m$ (11) | $P2_1/c$ (14) | $P\bar{1}$ (2) | $P\bar{1}$ (2) | $P\bar{1}$ (2) |
| $a$ [Å] | 8.9368(5) | 9.0756(3) | 7.4982(2) | 10.2124(5) | 9.1887(18) |
| $b$ [Å] | 10.6475(5) | 13.2900(4) | 11.7114(5) | 11.7804(5) | 11.601(2) |
| $c$ [Å] | 9.5294(5) | 14.5302(4) | 12.0123(5) | 14.1788(6) | 12.549(3) |
| α [deg] | 90 | 90 | 65.435(2) | 67.448(3) | 99.58(3) |
| $\beta$ [deg] | 115.403(3) | 98.718(2) | 84.890(2) | 75.255(3) | 93.84(3) |
| $\gamma$ [deg] | 90 | 90 | 75.842(2) | 65.836(3) | 94.50(3) |
| $V$ [Å$^3$] | 819.09(7) | 1732.31(9) | 930.14(6) | 1427.66(11) | 1310.6(4) |
| $Z$ | 2 | 4 | 2 | 2 | 2 |
| $\rho_{calcd}$ [g·cm$^{-3}$] | 1.744 | 1.749 | 1.679 | 1.885 | 1.956 |
| $\mu$ [mm$^{-1}$] | 2.117 | 2.008 | 1.872 | 2.553 | 2.591 |
| $F$(000) | 432 | 920 | 476 | 812 | 764 |
| crystal dimensions [mm] | 0.04 × 0.04 × 0.02 | 0.04 × 0.04 × 0.04 | 0.04 × 0.04 × 0.04 | 0.04 × 0.04 × 0.03 | 0.04 × 0.04 × 0.04 |
| 2$\theta$ range [deg] | 6.08−54.94 | 4.18−54.96 | 6.42−54.96 | 4.80−54.94 | 4.42−54.92 |
| index ranges | $-10 \le h \le 11$ | $-11 \le h \le 11$ | $-9 \le h \le 9$ | $-13 \le h \le 12$ | $-11 \le h \le 11$ |
| | $-13 \le k \le 13$ | $-16 \le k \le 17$ | $-15 \le k \le 12$ | $-15 \le k \le 15$ | $-15 \le k \le 13$ |
| | $-12 \le l \le 12$ | $-18 \le l \le 18$ | $-15 \le l \le 15$ | $-15 \le l \le 18$ | $-16 \le l \le 15$ |
| measured reflections | 5815 | 11846 | 6712 | 9688 | 9110 |
| unique reflections/$R_{int}$ | 1974/0.0438 | 3949/0.0355 | 4219/0.0229 | 6448/0.0325 | 5901/0.0324 |
| reflections used | 1974 | 3949 | 4219 | 6448 | 5901 |
| data with $I > 2\sigma(I)$ | 1540 | 3348 | 3512 | 5280 | 5231 |
| parameters | 111 | 208 | 217 | 327 | 334 |
| $S^a$ | 1.010 | 1.027 | 1.012 | 1.005 | 1.020 |
| $R_1$ [$I > 2\sigma(I)$]$^b$ | 0.0323 | 0.0280 | 0.0293 | 0.0340 | 0.0331 |
| $wR_2$ [all data, on $F^2$]$^c$ | 0.0780 | 0.0698 | 0.0698 | 0.0899 | 0.0919 |
| max./min residual electron density [e·Å$^{-3}$] | 0.536/−0.443 | 0.446/−0.564 | 0.355/−0.474 | 0.545/−0.615 | 0.778/−0.578 |
| CCDC No. | 697007 | 697008 | 697009 | 697011 | 697010 |

$^a$ $S = \{\sum[w(F_o^2 - F_c^2)^2]/(n-p)\}^{0.5}$; $n$ = no. of reflections; $p$ = no. of parameters. $^b$ $R_1 = \sum||F_o| - |F_c||/\sum|F_o|$. $^c$ $wR_2 = \{\sum[w(F_o^2 - F_c^2)^2]/\sum[w(F_o^2)^2]\}^{0.5}$.

**Reaction of 5b with $HBF_4 \cdot Et_2O$.** Compound **5b** (86 mg, 189 $\mu$mol) was dissolved in dichloromethane (3 mL), and the resulting solution was cooled to 0 °C. Subsequently, $HBF_4$ (51−57% in $Et_2O$) (26 $\mu$L, 189 $\mu$mol) was added, the mixture was stirred for 45 min at 0 °C, pentane (2 mL) was added, and the resulting solution was stored at −20 °C for 12 h. The formed precipitate was separated by filtration and washed with hexane (50 mL) to afford a red solid. IR (KBr): 2099 (vs), 2065 (vs), 2032 (vs), 1990 (vs).

**Reaction of 5b with Na/Hg.** In a 10 mL Schlenk vessel, compound **5b** (19 mg, 41.7 $\mu$mol) was dissolved in acetonitrile (5 mL), followed by the addition of sodium amalgam (0.2% Na in Hg), and the resulting two-phase system was shaken for 30 min. Within this time, the solution colored to dark red. Subsequently, this solution was investigated via IR spectroscopy under an argon atmosphere.

**Electrochemistry. Instrumentation and Procedures.** Cyclic voltammograms were recorded against a non-aqueous $Ag/Ag^+$ reference electrode (0.1 M [$n$-$Bu_4N$][$PF_6$] and 0.01 M $AgNO_3$ in acetonitrile) and Ag/AgCl using 0.45 M [$n$-$Bu_4N$][$BF_4$] in dichloromethane as the supporting electrolyte. A glassy carbon (GC) macroelectrode and a platinum wire were used as the working and auxiliary electrodes, respectively. A solution of 0.05 M [$n$-$Bu_4N$][$PF_6$] (Fluka, electrochemical grade) in acetonitrile (Aldrich, anhydrous, 99.8%) was used as the supporting electrolyte. Electrochemical experiments were carried out using a CHI750C electrochemical bipotentiostat. Prior to each experiment, the electrochemical cell was degassed for at least 10 min using argon, and a blanket of argon was maintained throughout. The GC working electrode was prepared by successive polishing with 1.0 and 0.3 $\mu$m alumina pastes and sonicated in Millipore water for 5 min. All cyclic voltammograms were recorded at a scan rate of 100 mV s$^{-1}$. In case of the studies of **5b**, cyclic voltammetric measurements were conducted in 3-electrode technique using a Reference 600 potentiostat (Gamry Instruments, Warminster, U.S.A.), which was controlled by DigiElch 5.R.[33] This program provides not only routines for the digital simulation of electrochemical experiments but also those for performing the measurements in a consistent way making use of the Gamry Electrochemical Toolkit library. Unless otherwise stated, the experiments were performed in acetonitrile (containing 0.25 M [$Et_4N$][$ClO_4$]) under a blanket of solvent-saturated argon. The ohmic resistance, which had to be compensated for, was determined by measuring the impedance of the system at potentials where the faradic current was negligibly small. Background correction was accomplished by subtracting the current curves of the blank electrolyte (containing the same concentration of supporting electrolyte) from the experimental CVs. The reference electrode was an Ag/AgCl electrode in acetonitrile containing 0.25 M [$n$-$Bu_4N$]Cl. However, all potentials reported in this paper refer to the ferrocenium/ferrocene couple, which was measured at the end of a series of experiments. The reduction processes were studied on a hanging mercury drop ($m_{Hg\text{-}drop} \approx 4$ mg) produced by a CGME instrument (Bioanalytical Systems, Inc.,West Lafayette, U.S.A.).

**Quantum Chemical Calculations.** The density functional programs provided by the TURBOMOLE 5.71 suite[34] were used for all calculations. The calculations were arranged with the density functional BP86[35,36] in combination with the resolution-of-the-identity (RI) technique[37] as implemented in TURBOMOLE. The BP86 functional is composed of the Becke exchange functional B88[35] and the Perdew correlation functional P86.[36] The preoptimizations of the geometries were

(33) DigiElch 5.R developed by M. Rudolph is available from http://www.gamry.com/Products/DigiElch5.htm

(34) Ahlrichs, R.; Bär, M.; Häser, M.; Horn, H.; Kölmel, C. *Chem. Phys. Lett.* **1989**, *162*, 165–169.

(35) Becke, A. D. *Phys. Rev. A* **1988**, *38*, 3098–3100.

(36) Perdew, J. P. *Phys. Rev. B* **1986**, *33*, 8822–8824.

performed with the basis set SVP.[38] The final structures and frequency calculations were calculated by applying the basis set TZVP.[39] The output IR line spectra were convoluted with a Gaussian profile of 15 $cm^{-1}$ width to better match the experimental spectra.

**Crystal Structure Determinations.** Compounds **5a**−**c**, **6b**, and **7** were crystallized from solutions in trichloromethane by slow evaporation of the solvent at 4 °C. The intensity data were collected on a Nonius Kappa CCD diffractometer using graphite-monochromated Mo−$K_\alpha$ radiation. Data were corrected for Lorentz and polarization effects but not for absorption.[40,41] Crystallographic data as well as structure solution and refinement details are summarized in Table 4.

The structures were solved by direct methods (SHELXS)[42] and refined by full-matrix least-squares techniques against $F_o^2$ (SHELXL-97).[42] All non-hydrogen atoms were refined anisotropically.[42] The hydrogen atoms were included at calculated positions according to the riding model.

**Acknowledgment.** Financial support for this work was provided by the Studienstiftung des Deutschen Volkes (U.-P.A.). Y.H. and J.G.V. thank the Science Foundation Ireland for financial support, Grant 06/RFP/029. We thank C. Robl and C. Burschka for valuable discussions in context with the crystal structure analyses. We also thank C. Apfel for comparison of the powder X-ray and the single-crystal X-ray diffraction data of **6a** and **6b**.

**Supporting Information Available:** Selected crystallographic data for **5a**−**c**, **6b**, and **7**, Raman spectrum of **6a**, additional discussion of the electrochemical properties of **5a**−**c**, and quantum chemical calculation of $\mathbf{5b}^{2-}\cdot CH_3CN$. This material is available free of charge via the Internet at http://pubs.acs.org.

**Note Added after ASAP Publication.** This paper was published on the Web on September 27, 2010, with the incorrect artwork for Figure 13. The corrected version was reposted on October 1, 2010.

(37) (a) Eichkorn, K.; Treutler, O.; Öhm, H.; Häser, M.; Ahlrichs, R. *Chem. Phys. Lett*. **1995**, *240*, 283–290. (b) Eichkorn, K.; Weigend, F.; Treutler, O.; Ahlrichs, R. *Theor. Chem. Acc*. **1997**, *97*, 119–124.
(38) Schäfer, A.; Horn, H.; Ahlrichs, R. *J. Chem. Phys*. **1992**, *97*, 2571–2577.
(39) Schäfer, A.; Huber, C.; Ahlrichs, R. *J. Chem. Phys*. **1994**, *100*, 5829–5835.
(40) *COLLECT, Data Collection Software*; Nonius B. V.: Delft, The Netherlands, 1998.
(41) Otwinowski, Z.; Minor, W. *Methods Enzymol*. **1997**, *276*, 307–326.
(42) Sheldrick, G. M. *Acta Crystallogr., Sect. A* **2008**, *64*, 112–122.